

# Chapter 8

## NSM Systems

**José Sena-Cruz, Joaquim Barros, Vincenzo Bianco, Antonio Bilotta, Dionysios Bournas, Francesca Ceroni, Glauca Dalfré, Renata Kotynia, Giorgio Monti, Emilio Nigro and Thanasis Triantafyllou**

**Abstract** This chapter gives an overview on the state-of-the-art of the Near-Surface Mounted (NSM) technique for structural retrofitting of reinforced concrete structures using Fibre Reinforced Polymers (FRP). The chapter is divided in 5 sections. Firstly, general aspects of the technique are introduced, including main advantages, nomenclature adopted, type of FRP reinforcement and adhesive used, groove geometry/location, and constructional aspects. Then, the existing

---

**Final Remarks** This chapter gave an overview about the current state of the near surface-mounted (NSM) strengthening technique. This technique presents high levels of efficiency for upgrading the flexural and shear carrying capacities of reinforced concrete (RC) structures. In the last decade several efforts were done to increase the knowledge in terms of bond, flexural, and shear responses of NSM systems. Some analytical formulations were proposed to predict its behaviour. Design rules were also presented. However, due to the limited number of experimental results, the existing formula have a limited application. In addition to that, there are several areas that need a lot of effort in order to appraise the response of NSM systems, such as durability and long-term behaviour.

---

J. Sena-Cruz (✉) · J. Barros  
University of Minho, Guimaraes, Portugal  
e-mail: jsena@civil.uminho.pt

V. Bianco · G. Monti  
Sapienza University of Rome, Rome, Italy

A. Bilotta · E. Nigro  
University of Naples Federico II, Naples, Italy

D. Bournas  
The University of Nottingham, Nottingham, UK

F. Ceroni  
University of Sannio, Benevento, Italy

G. Dalfré  
UNILA, Foz do Iguaçu, Brazil

R. Kotynia  
Lodz Technical University, Łódź, Poland

T. Triantafyllou  
University of Patras, Patras, Greece

© RILEM 2016

C. Pellegrino and J. Sena-Cruz (eds.), *Design Procedures for the Use of Composites in Strengthening of Reinforced Concrete Structures*, RILEM State-of-the-Art Reports 19, DOI 10.1007/978-94-017-7336-2\_8

knowledge on the bond behaviour is addressed focusing on the performed experimental investigations, results, and conclusions in terms of test setups, failure modes, and influence of different parameters on the bond performance. The performance of the existing local bond-slip behaviour laws, both proposed by codes and researches, is also addressed. Similar analysis is also followed for the case of flexural strengthening. The current state on shear strengthening includes two formulations for predicting the NSM shear carrying capacity. The chapter ends with a concluding section summarizing the current state and identifying the needs for future research.

**Keywords** FRP · Strengthening · NSM · Reinforced concrete

## Introduction

In early 2000s the near surface-mounted (NSM) strengthening technique was proposed and used as an alternative system to the externally bonded reinforcement (EBR). In the NSM the fibre reinforced polymer (FRP) reinforcements are inserted into pre-cut grooves opened in the concrete cover. The FRP is then fixed to concrete with an adhesive. The NSM concept is not new. In fact, in the 1940s it started to be used in Europe for the strengthening of reinforced concrete structures. This pioneering technique consisted on placing rebar into grooves located at the concrete cover. These grooves were then filled with cement mortar (Asplund 1949).

After more than 10 years of research and applications, the NSM strengthening technique has prevailed and, when compared with the EBR, presents the following main advantages (De Lorenzis and Teng 2007):

- The surface preparation is reduced and in some cases the amount of site installation work may be reduced;
- The removal of the weak concrete laitance layer is no longer needed;
- The levels of efficiency are higher since the technique is less prone to FRP debonding from the concrete substrate;
- The FRP reinforcements can be more easily anchored into adjacent members (preventing debonding failures);
- The FRP reinforcements are protected by the concrete cover and, consequently, are less exposed to mechanical damage, impact loading, fire and vandalism;
- The visual aspect of the strengthened structure is virtually unchanged.

Typically, glass FRP (GFRP) or carbon FRP (CFRP) are used as reinforcement materials. Depending on the cross-section geometry the FRP can be named by bar or strip (see Figs. 8.1 and 8.2). A FRP bar has square or round cross-section, whereas the FRP strip is characterized by a rectangular cross-section where the width is significantly higher than the thickness. Ribbed, sand-blasted, sand-coated,

smooth or spirally wounded are the most common external-surfaces of the bars, while smooth surface usually characterize the FRP strips.

Figure 8.1 shows the two most commonly tested and used solutions when the NSM strengthening technique is applied. In the FRP bars, the magnitude of groove width and depth,  $b_g$  and  $h_g$ , respectively, are similar. In general, to attain this type of grooves, two saw cuts and the removal of concrete between them with a chisel is required. In the case of FRP strips, narrow grooves are open in the concrete cover yielding to distinct magnitudes for the groove width and depth. Typically only one saw cut is required. The minimum values of groove dimensions recommended by ACI document (2008) are  $1.5d_b$  for both, in the case of bars, and  $3t_f$  and  $1.5w_f$ , for thickness and width, respectively, in the case of strips (see also Fig. 8.1).

Due to the final cross-section geometry of the grooves, square and rectangular FRP reinforcements explore it better than round FRP ones, since a uniform adhesive thickness is achieved. On the other hand, in round bars the normal stresses (perpendicular to the FRP) accompanying the tangential bond stresses (parallel to the FRP) tend to split the epoxy cover while in square and rectangular bars they act mainly towards the groove lateral concrete. Between these two, rectangular bars have been shown to be more efficient since they maximize the ratio of surface to cross-sectional area, which minimizes the bond stresses associated with a given tensile force in the FRP.

In the NSM system, the adhesive is responsible for stresses transfer between the FRP reinforcement and the concrete substrate. The main properties that affect the

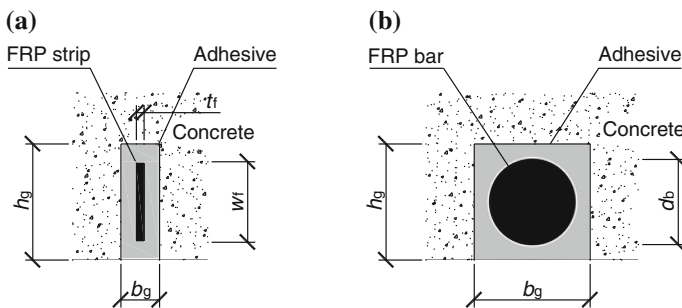


Fig. 8.1 NSM system using FRP a strip and b bar



Fig. 8.2 FRP systems

performance of the adhesive are its tensile and shear strength, modulus of elasticity and adhesion to the FRP. Up to now epoxy resins are the most frequently used adhesive; however, a few studies using cement mortar can be found.

The NSM application involves the following steps:

- a. Open grooves in the concrete cover using a saw cut machine;
- b. Clean the grooves with compressed air;
- c. Clean the FRP with an appropriate cleaner (e.g., acetone);
- d. Prepare the adhesive according to the supplier's recommendations;
- e. Fill the grooves and, if possible, cover the lateral faces of the FRP with the adhesive;
- f. Insert the FRP into the grooves, and slightly press it to force the adhesive to flow between the FRP and the grooves' borders. This phase requires a special care in order to assure that the grooves are completely filled with adhesive. When this is not the case the formation of voids might occur;
- g. Finally, the adhesive in excess is removed and the surface is levelled;
- h. The time of adhesive cure indicated by the supplier must be respected before its expected performance becomes fully available.

## Bond

In the present context, bond means the transfer of stresses between the concrete and the FRP reinforcement in order to develop the composite action of both materials, during the loading process of a concrete element. The bond performance influences the ultimate load carrying capacity of the reinforced element, as well as some serviceability aspects, such as crack width and crack spacing.

The bond strength of a NSM system is the maximum transferable load and is directly related to the type of failure (at the bar-adhesive interface, at the adhesive-concrete interface, within the concrete, cohesive at the adhesive and in the FRP material). The overall bond strength is dependent on local bond strength. In general, local bond strength is obtained from specimens with very short bond lengths or with large bond lengths where the strains (and/or slip) are measured. The local bond-slip behaviour is affected by the following main parameters: materials' mechanical properties, FRP reinforcement and grooves surface treatment, geometry of the strengthening system (bars or strips), grooves' dimensions and depth of the FRP reinforcement in the groove. The shape ratio,  $k$ , namely the ratio between groove and FRP dimensions, also affects the failure mode of the strengthening system (Sena Cruz and Barros 2004; De Lorenzis and Teng 2007; Seracino et al. 2007).

Experimental bond tests on concrete elements strengthened with NSM FRP bars or strips have been performed by several researchers during the last decade. In (De Lorenzis et al. 2004), GFRP and CFRP ribbed bars with 9.5 mm diameter and spirally wounded CFRP bars with 7.5 mm diameter were tested in concrete elements with mean compressive strength of 22 MPa. Most of the specimens failed by

adhesive splitting. In De Lorenzis and Nanni (2002), GFRP deformed bars (13 mm diameter) and CFRP deformed bars (9.5 mm diameter) were tested in concrete elements (27.5 MPa). All specimens failed by adhesive splitting. Moreover, sand blasted CFRP bars (9.5 and 13 mm diameter) were tested too and a FRP-adhesive interface failure occurred. In De Lorenzis et al. (2002) spirally wounded CFRP bars (7.5 mm diameter) were tested in concrete elements (22 MPa). All specimens attained an adhesive-concrete interface failure. In Sena Cruz and Barros (2004) and (Sena Cruz et al. 2006) smooth carbon strips with dimensions  $10 \times 1.4$  mm were tested in specimens characterized by three values of concrete strength (35, 45, and 70 MPa). Failure always occurred at the FRP-adhesive interface. In Seracino et al. (2007) smooth carbon strips with thickness of 1.2 mm and width of 10, 15, and 20 mm were tested. Concrete strength varied in the range 30–60 MPa. For the specimens with concrete strength equal or higher than 50 MPa a tensile failure of the FRP occurred, except for two cases which showed a FRP-adhesive interface failure. For lower values of strength, an adhesive-concrete interface failure was observed. In Teng et al. (2006) smooth carbon strips ( $16 \times 2$  mm) were tested in concrete specimens (44 MPa) and a FRP-adhesive interface failure occurred. In Novidis and Pantazopoulou (2008) sand blasted deformed CFRP bars (12 mm diameter) were tested in concrete specimens (30 MPa) and an adhesive-concrete interface failure was observed.

Regarding the setup, both numerical and experimental studies (Novidis and Pantazopoulou 2008) showed that different test setups can significantly change the experimental results. Nevertheless, at present, no consensus on a standard test procedure has been still reached. For this reason, a Round Robin initiative was recently carried out involving several research laboratories (En-Core and fib TG 9.3 2010; Palmieri et al. 2012) and aimed at testing the bond strength of the same FRP materials according to different setups in different laboratories. In particular, the laboratories of the Universities of Naples, Ghent, Minho and Budapest tested various NSM systems. All laboratories adopted a double shear test (DST), where two concrete blocks were connected by the NSM reinforcements on two opposite sides. The only exception was the laboratory of Naples (Bilotta et al. 2011), which used a single shear test (SST) setup. Failure modes were quite different; in particular in the tests carried out by the University of Minho an adhesive-concrete interface failure occurred in all cases, unless in the CFRP bars (6 mm diameter), which failed at the adhesive-FRP interface. In the tests performed at the University of Ghent, the failure happened at the FRP-adhesive interface for the smooth carbon bars (8 mm diameter) and for the thicker carbon strips ( $2.5 \times 15$  mm). Adhesive splitting occurred for both types of sand coated basalt bars and for the ribbed glass bars. In the other cases, an adhesive-concrete interface failure occurred. In most of the tests carried out by the University of Budapest failure occurred in the concrete block and only in some cases it was due to adhesive splitting. Finally, a concrete-adhesive interface failure occurred in most specimens strengthened with NSM systems at the University of Naples. Even if the DST setup led, in some cases, to the failure of the concrete due to an incorrect alignment of the two blocks, it is worth noting that the concrete strength could affect the failure mode. Indeed concrete strength varied

in the range 27–32 MPa for the tests at University of Ghent, was 43 MPa at University of Budapest and 35 MPa at University of Minho. At the University of Naples, a lower concrete strength (about 19 MPa) was used in order to replicate the conditions of existing RC buildings. For low strength, a concrete cohesive failure is more probable.

Based on the collected experimental results, the possible failure modes can be defined as:

**i. Debonding at FRP bar/strip—adhesive interface**

A pure interfacial mode can be critical for bars with a smooth or lightly sand-blasted surface (De Lorenzis and Nanni 2002), i.e. when the bond resistance relies primarily on the adhesion between the bar and the adhesive. This type of failure is identified by the virtual absence of adhesive attached to the bar surface after failure. For round bars, longitudinal cracking of the adhesive cover produced by the radial components of the bond stresses may accelerate the occurrence of an interfacial failure.

**ii. Cohesive shear failure within the adhesive**

The cohesive shear failure of the adhesive was observed for strips with a roughened surface (Blaschko 2003). Such a failure is identified by the presence of adhesive on both strip and concrete after failure and occurs when the tensile strength of the adhesive is exceeded. Since surrounding concrete is much stiffer than the adhesives, it introduces some confinement at the concrete-adhesive interface. Therefore, the Mohr-Coulomb principles contribute to avoid a pure sliding failure mode at the concrete-adhesive interface and induce the failure within the adhesive.

**iii. Debonding at adhesive—concrete interface**

Bond failure at the adhesive-concrete interface may occur as pure interfacial failure or as cohesive shear failure in the concrete. The pure interfacial failure mode was found to be critical for pre-cast grooves (De Lorenzis et al. 2002) and, in general, for grooves with smooth surfaces. Indeed, in this case the cohesion/adhesion phenomena are very small, as well as the internal friction angle of the materials in contact, therefore the shear strength at the interface due to the Mohr-Coulomb effect is small, being the weakest link of the all system. Cohesive shear failure within the concrete is the most common failure mode since concrete is the weakest material. Indeed, the surrounding concrete at the loaded end is subjected to tensile stresses that exceeds the tensile strength of the concrete, as long as the bond length is long enough (Ceroni et al. 2012). It has been observed also in bond tests on concrete specimens strengthened with smooth NSM strips (Seracino et al. 2007). In general, the failure at the adhesive-concrete interface was experimentally observed for values of the shape factor  $k > 1.5$ –2 (De Lorenzis and Teng 2007); these limits, indeed, warrant a sufficient adhesive thickness around the FRP bar/strip in order to avoid the adhesive cover splitting.

**iv. Adhesive cover splitting**

Longitudinal cracking of the adhesive is generally identified as cover splitting. This was observed to be the critical failure mode for deformed (i.e. ribbed and spirally wound) round bars in moderate strength concrete (De Lorenzis and Nanni 2002; De

Lorenzis et al. 2004). Specimens with low values of groove size ( $k \approx 1$ ) and very brittle adhesive can show its splitting without significant damage in the surrounding concrete. For increasing groove depth and adhesive thickness, the resistance of the adhesive cover to splitting increases and failure is controlled by cracking of the surrounding concrete: in these cases the bond strength can also increase with the groove size until the failure load corresponding to the adhesive-concrete interface failure is attained. Moreover, as deeper the FRP is installed into the groove as larger confinement the surrounding concrete introduces to the FRP, resulting in beneficial effects in terms of bond strength (Costa and Barros 2011). A minimum value of  $k = 1.5$  is suggested to avoid splitting (De Lorenzis and Nanni 2002). Splitting failure is also typical of specimens strengthened with cement filled grooves for low values of the  $k$  factor, due to the lower tensile strength of the cement fillers.

#### v. Concrete splitting

When an NSM bar/strip is close to the edge of a concrete member, failure can involve the splitting of the edge concrete (Blaschko 2001; Galati and De Lorenzis 2009). This kind of failure mode can be easily eliminated by keeping a minimum distance from the edge. Moreover this kind of failure can be quite common mainly in elements of relatively low strength class.

### *Evaluation of the Existing NSM ACI Formulation*

The ACI 440.2R-08 (2008) guide includes a simple formulation for predicting the maximum pullout strength. In this formulation the key parameter is the maximum bond strength for the entire NSM system. If the bonded length ( $L_b$ ) is at least equal to a development length ( $L_d$ ), then the experimental bilinear shear stress versus slip law can be assumed to be constant along the bond length and equal to the average bond strength ( $\tau_{avg}$ ). ACI assumes  $\tau_{avg}$  equal to 6.9 MPa for all FRP NSM systems. Hence, by imposing this limit  $\tau_{avg}$  to the connection's maximum capacity,  $L_d$  and the maximum pullout force installed in the FRP ( $F_{f,max}$ ) can be estimated. Then, if  $L_b \geq L_d$  the failure will occur by FRP rupture. Otherwise it will occur by one of the five failure modes described in the previous section.

It is interesting to notice that only four parameters need to be known *a priori* in order to predict  $F_{f,max}$  using ACI formulation, namely: FRP perimeter ( $p_f$ ), cross-section area ( $A_f$ ), tensile strength ( $f_{fu}$ ), and bonded length ( $L_b$ ).

$$L_d = \frac{A_f f_{fu}}{p_f \tau_{avg}} \quad (8.1)$$

$$F_{f,max} = \begin{cases} A_f f_{fu} & \text{if } L_b \geq L_d \\ A_f f_{fu} \frac{L_b}{L_d} & \text{if } L_b < L_d \end{cases} \quad (8.2)$$

**Fig. 8.3** Comparison between the experimental ( $F_{f,max\_Exp}$ ) and ACI numerical ( $F_{f,max\_Num}$ ) maximum pullout force prediction

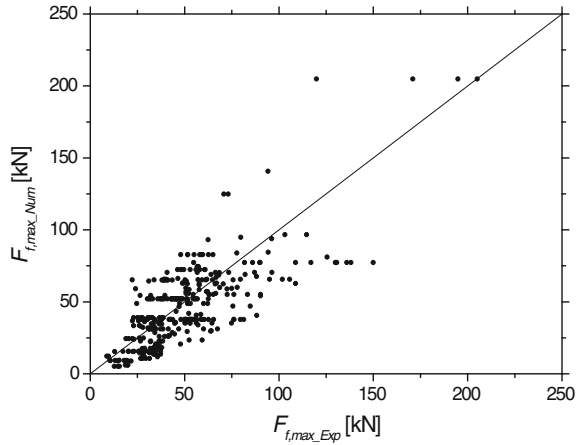
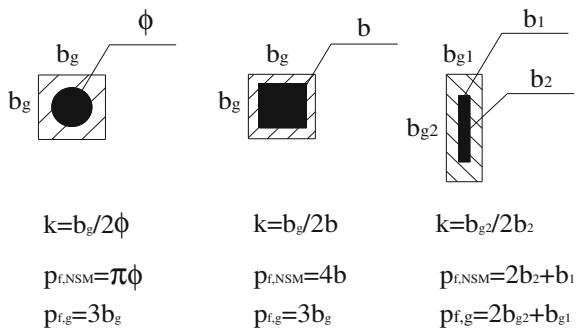


**Fig. 8.4** Definition of geometrical parameters of the grooves



An ongoing analytical work is being performed in order to assess the accuracy of ACI formulation (Coelho et al. 2013, 2014). Preliminary results from a database with 363 direct pullout tests using different setups and materials are shown in Fig. 8.3.

As can be seen, a large scatter exists which is also verified by computing the error measures associated to the ratio between numerical and experimental values of the maximum pullout force. A standard variation of 0.4 was found, corresponding to a coefficient of variation of almost 42 %. This reveals that further improvements are needed for the ACI NSM formulation.

### Predicting Formulae for NSM

A reference database of 167 results from bond tests available in the literature (93 tests on round bars, 12 on square bars, and 62 on rectangular strips) were collected. Figure 8.4 and Table 8.1 show the ranges of the main geometrical and mechanical parameters of the FRP NSM systems used in the tests. Note that the groove dimensions are compatible with the usual concrete cover values.



**Table 8.1** Ranges of geometrical and mechanical parameters of the experimental database

Geometry	FRP	Groove
93 round bars (mm)	$\varnothing = 6\div 10$	$b_g = 10\text{--}25$
12 square bars (mm)	$b = 10$	$b_g = 15$
62 strips (mm)	$b_1 = 1.2\text{--}2.5$ $b_2 = 10\text{--}20$	$b_{g1} = 3.3\text{--}8$ ; $b_{g2} = 12\text{--}25$
Concrete	Strength $f_{cm}$ (MPa)	19–70
FRP	Youngs' modulus (GPa)	37–182

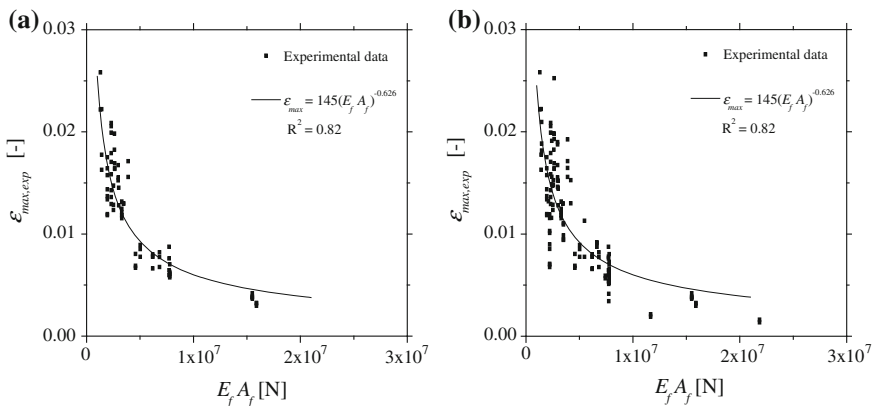


**Fig. 8.5** Experimental maximum strain for bond failure versus  $E_f \cdot A_f$ : **a** experimental results in the case of A/C failure; **b** extended database for different types of bond failure modes

An approach to have a design formulation for the maximum strain at failure in the FRP reinforcement consists in extrapolating a trend based on experimental measures of strain at failure. Thus, the maximum experimental strain calculated dividing the failure load to the reinforcement axial stiffness,  $E_f \cdot A_f$ , is plotted in Fig. 8.5a versus the axial stiffness itself for the experimental results of the bond tests of (De Lorenzis et al. 2002, 2004; Seracino et al. 2007; En-Core and fib TG 9.3 2010; Bilotta et al. 2011, 2012), where an adhesive-concrete interface failure (A/C) occurred (totally 78 data). Figure 8.5a shows that the maximum strain decreases as the axial stiffness increases, as well as usually observed for the EBR systems (Triantafyllou and Antonopoulos 2000). The following law is able to fit the experimental results ( $R^2 = 0.82$ ):

$$\epsilon_{\max,th} = a \cdot \frac{1}{(E_f \cdot A_f)^b} \tag{8.3}$$

where  $a = 145$  and  $b = 0.625$  clearly depend on the database used for the regression.

Indeed, in Fig. 8.5b further experimental data (De Lorenzis and Nanni 2002; Sena Cruz and Barros 2004; Sena Cruz et al. 2006; Teng et al. 2006) were added to

**Table 8.2** Regression coefficients of Eqs. (8.3) and (8.4) for different sets of experimental results

Eq.	Database	Failure mode	a	b	c	R <sup>2</sup>
(8.3)	78 data	A/C	145	0.625	–	0.82
	137 data	A/C, A/F, S	112	0.61	–	0.66
(8.4)	78 data	A/C	145	0.74	0.45	0.85
	137 data	A/C, A/F, S	272	0.85	0.71	0.76

take into account also the results of specimens where adhesive-FRP interface failure (A/F) or splitting failure of the adhesive (S) occurred (totally 137 data). These data have been plotted together because the latter two failure modes can be, however, considered as ‘bond’ failures. The graph shows, as expected, a reduction of  $R^2$  due to the higher scatter of the experimental results characterized by several types of bond failure modes ( $R^2 \approx 0.66$ ). For the extended database, the best fitting regression coefficients are  $a = 112$  and  $b = 0.61$ . In Table 8.2 the values of  $a$  and  $b$  for the two sets of experimental results are listed.

In order to take into account the effect of the groove perimeter,  $p_{f,g}$ , the expression for the maximum strain has been modified as follows:

$$\varepsilon_{\max,th} = a \cdot \frac{(p_{f,g})^c}{(E_f \cdot A_f)^b} \quad (8.4)$$

The regression coefficients  $a$ ,  $b$  and  $c$  have been evaluated according to a least-square best fitting criterion for the same sets of data used for assessing the coefficients of Eq. (8.3). In Table 8.2 the values of these coefficients are listed together with the corresponding value of  $R^2$ .

When only the A/C interface failure modes are considered, a slight improvement of the experimental-theoretical fitting is achieved as evidenced by the  $R^2$  values (0.82 for Eq. (8.3) and 0.85 for Eq. (8.4)). By contrast, when the regression is extended to the whole database (137 data) considering different failure modes, a sensible improvement is obtained using Eq. (8.4):  $R^2 = 0.76$  for Eq. (8.4) versus  $R^2 = 0.66$  for Eq. (8.3). In Fig. 8.6 the experimental strain at failure is compared with the provisions given by Eq. (8.4) where the best fitting values of coefficients calibrated on the extended database are used (137 data for different types of bond failure modes).

Another parameter that might influence the maximum strain is the concrete compressive strength. This effect has been investigated too for the available data, but no clear influence was evidenced for now. Therefore, using Eq. (8.4) is preferable with respect to Eq. (8.3) due to the higher  $R^2$  of the regression on all sets of experimental data considered.

In Fig. 8.7 are shown the predictions given by Eq. (8.4) when coefficients calibrated on 78 and 137 data are used. To make the comparison, a value of the perimeter  $p_{f,g} = 40$  mm has been fixed, by taking into account that it generally varies between 20–60 mm, with an upper bound due to the ordinary values of

**Fig. 8.6** Experimental maximum strain versus theoretical values given by Eq. (8.4) calibrated on the extended database (137 data)

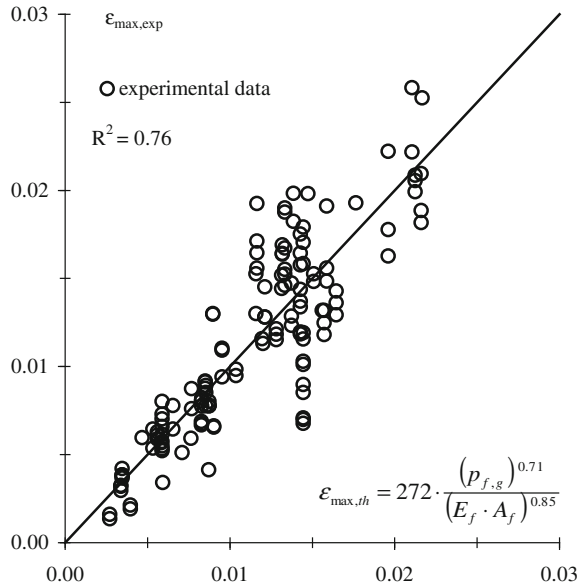
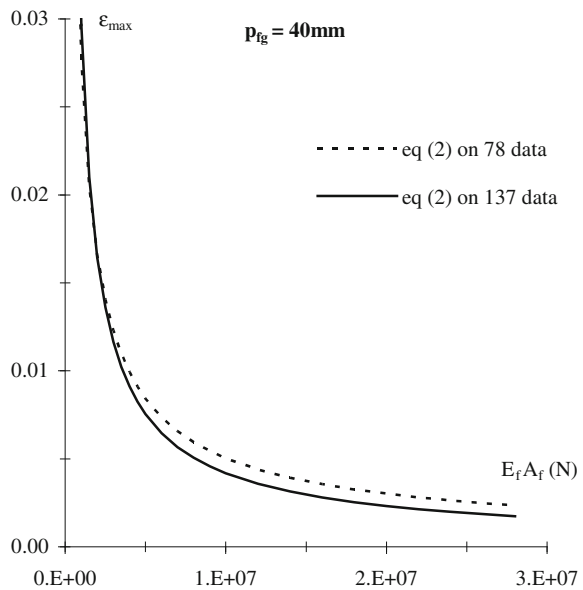


**Fig. 8.7** Theoretical prediction by Eq. (8.4) for  $p_{f,g} = 40$  mm



concrete cover (20–30 mm). It is clear that the Eq. (8.4) with coefficient calibrated on 78 data provides predictions higher than those obtained on 137 data (i.e. +10–20 %). Similar results are obtained for different perimeters: as lower the value of  $p_{f,g}$  as larger the differences between the predictions. However, the less conservative formula can be used only if a failure at the interface A/C is expected. Hence, aimed

at giving design provisions, using the most conservative formula is preferable, because not sure indications are available to avoid failure modes in the adhesive (splitting or debonding at FRP-adhesive interface). Note that in the experimental database the parameter  $p_{f,g}/p_{f,NSM}$  varies between 1.2 and 2.5. So the formula given by Eq. (8.4) should be used for values of  $p_{f,g}/p_{f,NSM}$  ranging in this interval.

To finalize, it should be stressed that Eqs. (8.3) and (8.4) give average values of the maximum strain in the FRP reinforcement, whereas a characteristic value has to be estimated to give design provisions.

## Flexural Strengthening

### Beams and Slabs

When the NSM is used for flexural strengthening, the most common FRP reinforcement used consists of bars (circular and square cross-section) or rectangular strips (Fig. 8.8).

The existing experimental tests on RC members strengthened in flexure with NSM FRP reinforcement contain RC beams (De Lorenzis et al. 2000; Blaschko 2001; Hassan and Rizkalla 2003; Täljsten et al. 2003; EI-Hacha and Rizkalla 2004; Barros and Fortes 2005; Teng et al. 2006; Barros et al. 2007; Castro et al. 2007; Kotynia 2007a; Novidis and Pantazopoulou 2007; Yost et al. 2007; Burke 2008; Kalayci 2008; Al-Mahmoud et al. 2009; Costa and Barros 2010) and slabs

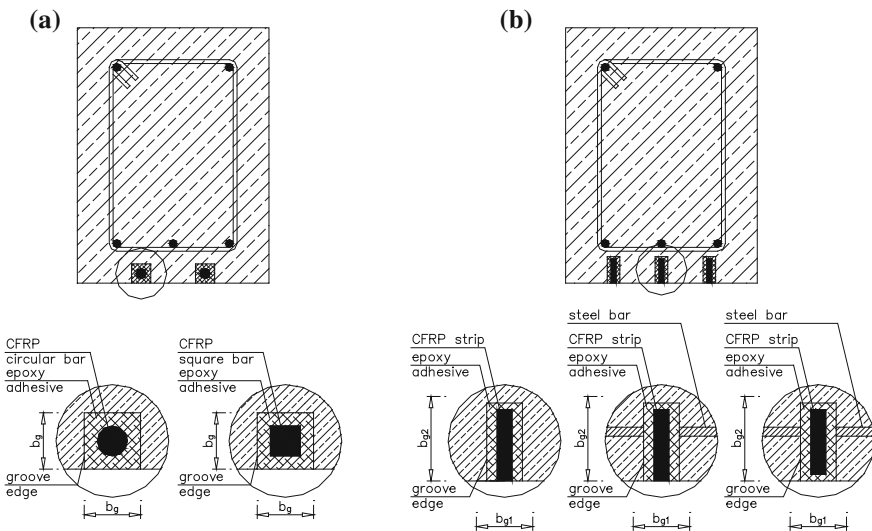


Fig. 8.8 Flexural strengthening of RC members with: **a** NSM bars and **b** strips

(Asplund 1949; Liu et al. 2006; Bonaldo et al. 2008; Dalfré and Barros 2011). The test database collected for analysis refers almost 50 RC members strengthened with NSM FRP. More than 80 % of them contain beams and only less than 20 % slabs.

The most popular FRP reinforcement used for NSM strengthening is made of CFRP (with more than 70 % for strips and 20 % for bars), there are only 8 % of members strengthened with GFRP bars. The tested specimens differ in geometry, load and static schemes, internal steel reinforcement ratio, NSM FRP percentage, FRP shape, its cross-section, concrete and adhesive strengths, concrete cover thickness and size of RC members.

Based on published research in the field of flexural strengthening with NSM FRP bars/strips, the most interesting observations are described and discussed in the following paragraphs.

De Lorenzis et al. (2000) conducted one of the first tests on RC T-section beams strengthened with CFRP and GFRP bars. Test results indicated increase in the ultimate load of the strengthened specimens in comparison with the reference ones. Also, they showed that the efficacy of the NSM technique depends on the bond length of the NSM reinforcement.

Täljsten et al. (2003) tested rectangular beams in four point bending test configuration. Two different dimensions of square grooves with 10 mm for cement grout and 15 mm for epoxy grout were used. Rupture of the rods occurred in the beam with the epoxy adhesive while FRP-adhesive slipping occurred in the beam with the cement grout.

Hassan and Rizkalla (2003) carried out bond tests on nine T-section RC beams strengthened with NSM CFRP strips with variable embedment lengths. The maximum strain of the CFRP bars ranged from 0.7 to 0.8 % for embedment lengths below 800 mm. Results showed an increase in the CFRP strain during its debonding with the increase in the embedment length. Failure of the beams with ribbed NSM FRP round bars occurred by splitting of the adhesive which occurred due to CFRP bond length below 800 mm. Whereas, in the case of beams strengthened with NSM strips, rupture of the strips occurred when the embedment length was larger than 850 mm.

EI-Hacha and Rizkalla (2004) tested T-section beams strengthened with CFRP strips or bars and thermoplastic GFRP strips in three point bending test. The use of NSM FRP reinforcements enhanced the flexural stiffness and significantly increased the ultimate load-carrying capacity of strengthened specimens. FRP-adhesive splitting was the dominant failure mode for the beams strengthened with NSM CFRP bars as a result of the high tensile stresses at that interface.

Barros and Fortes (2005) and Barros et al. (2007) investigated RC beams strengthened in flexure with variable number of NSM CFRP strips and different steel reinforcement ratios. Test results indicated an almost double increase in the load carrying capacity. Significant increases in the load at steel yielding and concrete cracking points for the strengthened beams, proved the higher efficiency of the NSM technique in comparison with EBR one.

Teng et al. (2006) investigated the influence of the embedment length of the strip. Test results of the beams strengthened with the shortest embedment length of

500 mm confirmed no effect of the strengthening on the ultimate load and on the beam's stiffness. The medium embedment length beams, ranging from 1200 to 1800 mm, indicated increases in the load bearing capacity. Those beams failed by concrete separation starting from the cut-off region towards the maximum moment region. Finally, the longest embedment length showed the propagation of debonding from the maximum moment region towards the cut-off section.

The results of 12 T-section RC beams by Castro et al. (2007) indicated failure due to intermediate crack debonding in the beams strengthened with CFRP strips and GFRP bars. Beams strengthened with CFRP bars failed by the bar-adhesive slipping.

Novidis and Pantazopoulou (2007) confirmed very promising results of the NSM technique in comparison to the EBR. The results indicated that the depth at which the FRP is bonded into the longitudinal grooves influences the strengthening gain.

Kotynia (2007a) tested three series of RC beams strengthened with NSM CFRP strips. The influence of the following parameters on the strengthening efficacy was investigated: CFRP depth, concrete cover thickness, longitudinal tensile steel, CFRP percentages, and concrete strength. Cutting of the steel stirrups in the tensile zone of the beam during the strips application did not influence the ultimate load capacity.

Based on 12 specimens, Kalayci (2008) investigated the influence of the groove size on the strengthening gain. The beams were tested with one type of strip/bar bonded into three different groove sizes. The ultimate loads reached for undersized groove specimens strengthened with CFRP strips was similar to the loads in the control specimens, even though the mid-span deflections were lower. Undersized and control groove beams had identical modes of failure: concrete and adhesive splitting. However, in the oversized specimens only concrete splitting occurred. Beams strengthened with CFRP bars reached similar deflections and ultimate loads in the control and undersized grooves specimens but, in the undersized specimens, adhesive splitting failure was observed. One of the oversized specimens failed by adhesive splitting while the other one by concrete splitting. Tests showed that smaller grooves led to adhesive splitting failures and bigger ones led to concrete splitting failures.

All the tests mentioned showed a significant effect of the FRP and steel reinforcement ratios likewise CFRP elasticity modulus on the ultimate loads and the CFRP strain utilization. The increase in the CFRP stiffness led to an ultimate load increase. However, it causes a decrease in the CFRP debonding strain.

## Failure Modes

Fundamental division of the test specimens refers to the failure mode. The most expected failure mode is the intermediate crack (IC) debonding with the adjacent concrete cover separation and FRP rupture, which clearly show the full FRP strain utilisation. While the adhesive splitting (AS) or concrete crushing (CC) have been confirmed as premature failure modes, which do not indicate attractive

strengthening efficiency. The AS failure with the FRP debonding from the adhesive indicates a low strength of the adhesive and strongly depends on the adhesive tensile strength (which, for this failure mode, is lower than the concrete strength) and the groove size (for higher groove widths adhesive splitting is observed more often).

The following failure modes appeared in the experimental tests of the RC members strengthened in flexure with NSM FRP reinforcement and are considered in the analysis of the strengthening efficiency:

*Interfacial debonding*

Interfacial debonding or adhesive cover splitting at the FRP-adhesive interface near the anchorage zone observed in the RC members NSM strengthened in flexure referred to similar failure modes observed in the bond tests.

*Concrete cover separation*

Concrete cover separation is more common for RC members strengthened with lower distances between the several grooves of the strengthening system since this can lead to a undesirable group effect. This is also more frequent for decreasing tensile strengths of the concrete cover.

In many tests (Asplund 1949; De Lorenzis et al. 2000; Barros and Fortes 2005; Barros et al. 2007; Kotynia 2007a; Bonaldo et al. 2008) bond cracks inclined at approximately  $45^\circ$  to the beam axis formed on the soffit of the beam. Upon reaching the edges of the beam's soffit, these cracks may propagate upwards on the beam sides maintaining a  $45^\circ$  inclination within the cover thickness. Then, they can propagate horizontally at the level of the steel tension bars.

**(a) Bar/strip end cover separation**

Concrete cover separation is typical for the extremities of NSM FRP reinforcement at a significant distance from the supports. This failure starts from the cut-off section and propagates to the midspan of the RC member (Teng et al. 2006; Barros et al. 2007; Al-Mahmoud et al. 2009; Costa and Barros 2010) (Fig. 8.9).

**(b) Localized cover separation**

Bond cracks within or close to the maximum moment region together with pre-existing flexural and/or flexural-shear cracks may isolate triangular or

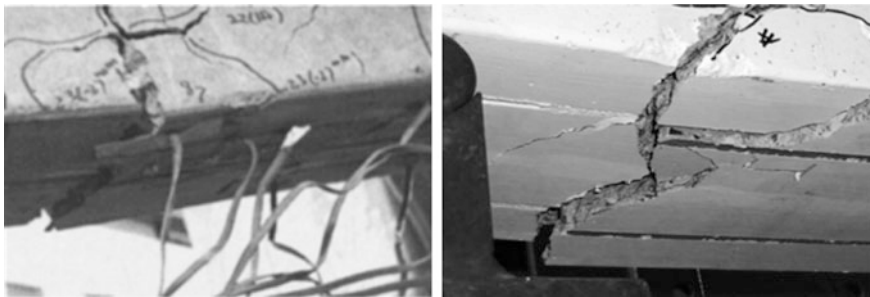


**Fig. 8.9** Failure by strip end cover separation (Teng et al. 2006; Costa and Barros 2010)

trapezoidal concrete wedges. From those, one or more will eventually split off (Barros et al. 2007; Costa and Barros 2010).

**(c) Flexural crack-induced cover separation**

This failure mode is similar to the intermediate crack debonding in reinforced concrete members externally bonded with FRP materials. Concrete cover separation is followed by flexural concrete cracking propagating along the NSM reinforcement, involving one of the shear spans and the maximum bending moment region (De Lorenzis et al. 2000; Barros and Fortes 2005; Barros et al. 2007; Kotynia 2007a; Bonaldo et al. 2008; Costa and Barros 2010) (Fig. 8.10).

**(d) Flexural-shear crack-induced cover separation**

Similar to the EBR technique, when diagonal shear crack intersects the FRP, debonding initiates due to shear and normal interfacial stresses on the side of the crack and propagates towards the FRP reinforcement end. The failure generates in the concrete adjacent to the adhesive-concrete interface and promotes the concrete cover separation (Fig. 8.11a) (Costa and Barros 2010; Dalfré and Barros 2011).

When using NSM with the high depth strips, a longitudinal fracture along the strip can be formed due to the relatively high moment of inertia, which leads to the fracture along the FRP strip (Fig. 8.11b) (Costa and Barros 2010).

**(e) Beam edge cover separation**

Failure mode typical when the FRP NSM bar is located near the beam's edge. Detachment of the concrete cover appears along this edge (Fig. 8.12).

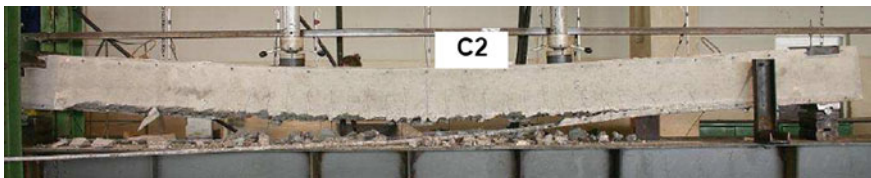


**Fig. 8.10** Failure by intermediate crack debonding with adjacent cover concrete (Kotynia 2007a)

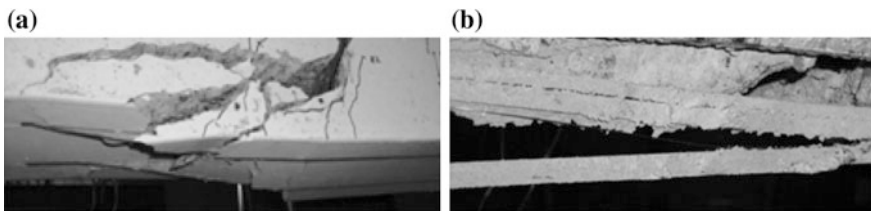


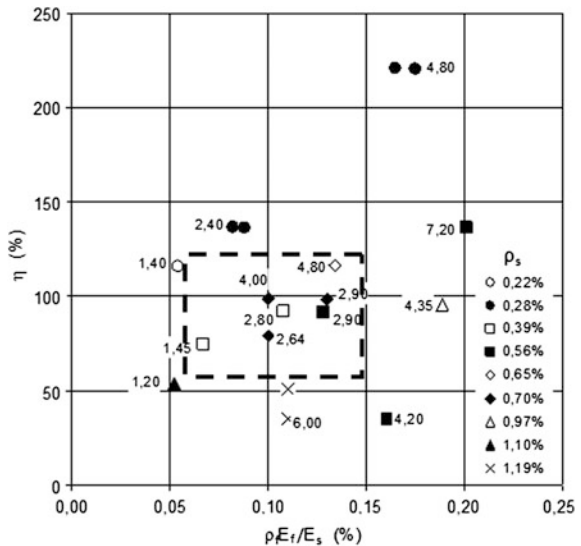
**Fig. 8.11** Failure by concrete cover separation: **a** Followed by flexural shear failure crack propagation; **b** Fracture along the NSM strip (Costa and Barros 2010)





**Fig. 8.12** Failure by the beam edge concrete cover separation (De Lorenzis and Teng 2007)

**Fig. 8.13** Effect of the equivalent FRP percentage on the strengthening ratio (values of parameter  $A_f/b_f$  describe test result) (Cholostiakow et al. 2013)



**Influence of Different Parameters on the Flexural Strengthening Performance**

To unify the test results and to preserve the highest NSM efficiency in terms of the FRP tensile strain utilization and the gain of the ultimate load, only the specimens which failed due to concrete cover separation (CCS) were taken into analysis. The first parameter taken into consideration was the equivalent FRP reinforcement ratio expressed by  $\rho_{f,eq} = \rho_f E_f / E_s$ . The influence of the equivalent FRP ratio on the strengthening ratio ( $\eta_f$ ) is shown on Fig. 8.13. The collected test data was divided into several series with longitudinal steel reinforcement ratios,  $\rho_s$ , ranging from 0.22 to 1.19 %. Moreover, the FRP cross section to its depth/width ratio, expressed by parameter  $A_f/b_f$ , identifies each test result (with values written next to the test results on Fig. 8.13). This figure indicates that specimens with similar steel ratio show increase in the strengthening ratio ( $\eta_f$ ) with increase in the strengthening ratio

( $\rho_{f,eq}$ ). It should be noted that the strengthening efficiency increases with a decrease in the internal steel ratio (Cholostiakow et al. 2013).

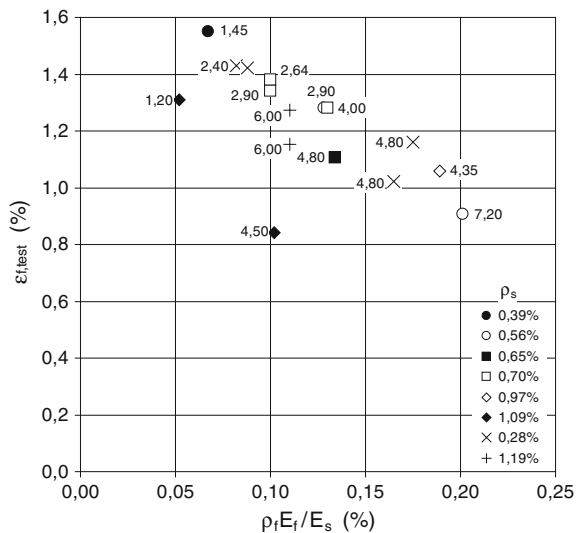
The highest strengthening ratio of 221 % was obtained for the steel ratio  $\rho_s = 0.28 \%$ , whereas the lowest strengthening ratio of 35 % was obtained for steel ratios of 1.19 and 0.56 %. It seems that the most effective NSM FRP strengthening was obtained in cases of RC members reinforced with steel ratios in the range of 0.38–0.71 % which are strengthened with the equivalent FRP reinforcement ratios in the range 0.07–0.15 %.

The data corresponding to the most effective NSM FRP strengthening cases are presented in the area confined with a dashed line (Fig. 8.13). For this region of effective strengthening combinations it can be said that a minimum of 2.6 mm for the ratio  $A_f/b_f$  is necessary.

The results indicate that with an increase of this parameter, the strengthening ratio increases. Moreover,  $A_f/b_f$  parameter has a crucial influence on the maximum FRP maximal strain,  $\epsilon_{f,test}$ , during failure of the RC specimens by CCS. Test results confirm that  $\epsilon_{f,test}$  is not affected by both the concrete strength and steel reinforcement ratio. Whereas the equivalent FRP reinforcement ratio,  $\rho_{f,eq}$ , has significant effect on the FRP strain utilization.

Comparison between beams strengthened with NSM FRP strips and bars shows a more significant decrease in the strengthening ratio for beams strengthened with bars than for beams strengthened with strips. A decrease in the FRP strain  $\epsilon_{f,test}$  with an increase in the equivalent FRP ratio is clearly visible in Fig. 8.14. Most of tested beams failed due to the CCS at the maximum NSM FRP strains in a range of 1.2–1.4 %. Test results show an inverse relation between the FRP strain and the parameter  $A_f/b_f$  that lead to the higher FRP strain utilization for lower values of that ratio.

**Fig. 8.14** Effect of equivalent FRP ratio on maximal strain in CFRP strips with values of a parameter  $A_f/b_f$  next to test results (Cholostiakow et al. 2013)



Basically, increase in the FRP stiffness causes decrease in the maximum FRP strain  $\epsilon_{f, test}$ . Moreover this observation corresponds to a tendency of decreasing strain efficiency with increasing the equivalent FRP reinforcement ratio  $\rho_f E_f / E_s$ .

Also the shape of the FRP cross-section (rectangular, square, or circle) and its position (horizontal or vertical) strongly affect the FRP strain efficiency  $\epsilon_{f, test}$  registered in the tests (Cholostiakow et al. 2013).

### Flexural Strengthening According to ACI 440.2R-08 versus Experimental Results

The ACI 440.2R-08 design guideline presents guidance on the calculation of the flexural strengthening effect of adding longitudinal NSM FRP reinforcement to the tension face of a reinforced concrete member. A specific illustration of the concepts applied in this section to the strengthening of existing rectangular or T-section RC members in the tension zone with non-prestressed steel is given on Fig. 8.15.

The following assumptions are made when calculating the flexural resistance of a section strengthened with an externally applied FRP system:

- Design calculations are based on the dimensions, internal reinforcing steel arrangement, and material properties of the existing member being strengthened;
- The strains in the steel reinforcement and concrete are directly proportional to the distance from the neutral axis (plane section principle);
- There is no relative slip between external FRP reinforcement and the concrete;
- The shear deformation within the adhesive layer is neglected because the adhesive layer is very thin with slight variations in its thickness;
- The maximum usable compressive strain in the concrete is 0.003;
- The tensile strength of concrete is neglected and the FRP reinforcement has a linear elastic stress-strain relationship until failure.

Unless all loads on a member, including self-weight and any prestressing forces, are removed before installation of FRP reinforcement, the substrate to which the FRP is applied will be strained. These strains should be considered as initial strains and should be excluded from the FRP strain.

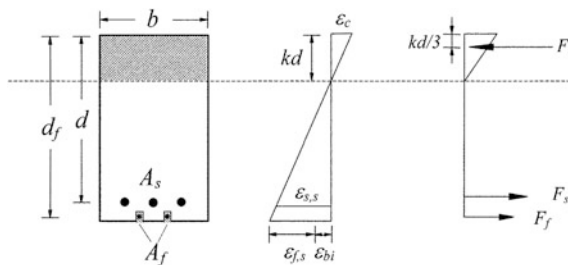


**Fig. 8.15** Elastic strain and stress distribution in the RC members strengthened in flexure with NSM FRP reinforcement (ACI 2008)

The initial strain level on the bonded substrate,  $\epsilon_{bi}$ , can be determined from an elastic analysis of the existing member, considering all loads that will be on the member during the installation of the FRP system. The elastic analysis of the existing member should be based on cracked section properties.

The maximum strain level that can be achieved in the FRP reinforcement will be governed by either the strain level developed in the FRP at the point at which concrete crushes, the point at which the FRP ruptures, or the point at which the FRP debonds from the substrate. The effective strain level in the FRP reinforcement at the ultimate limit state  $\epsilon_{fe}$  can not exceed the effective design strain for FRP reinforcement at the ultimate limit state  $\epsilon_{fd}$ .

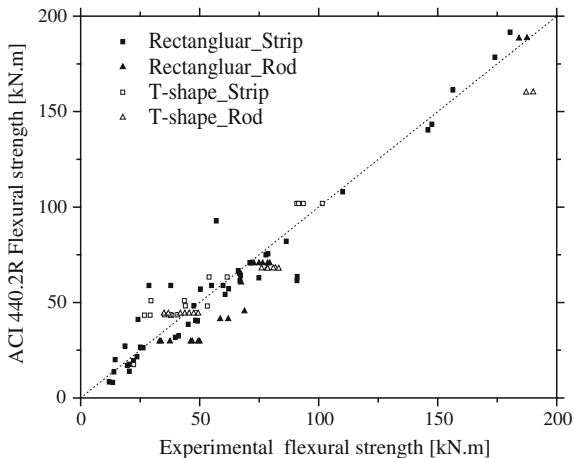
For NSM FRP applications, the value of  $\epsilon_{fd}$  may vary from 0.6 to 0.9  $\epsilon_{fu}$  depending on many factors such as member dimensions, steel and FRP reinforcement ratios and surface roughness of the FRP bar. Based on existing studies the committee recommends the use of  $\epsilon_{fd} = 0.7 \epsilon_{fu}$ . To achieve the debonding design strain of NSM FRP bars  $\epsilon_{fd}$ , the bonded length should be greater than the development length.

The design strategy explained above was applied to a database of RC beams under the following assumptions: ACI unit safety coefficients, mean material properties, steel in compression accounted, and parabola-rectangle concrete diagram with  $\epsilon_{cu} = 3.0 \text{ ‰}$  (Dias et al.) (Fig. 8.16).

### Continuous RC Slabs

The Externally Bonded Reinforcement (EBR) and the Near Surface Mounted (NSM) are the most used FRP-based techniques for the strengthening of RC elements. The efficiency of the NSM technique for the flexural and shear strengthening

**Fig. 8.16** Comparison between experimental and ACI prediction of the flexural strength (Dias et al.)



of RC members has already been assessed. However, most of the tests were carried out with NSM strengthened simply supported elements. Although many in situ RC strengthened elements are of continuous construction nature, there is a lack of experimental and theoretical studies in the behaviour of statically indeterminate RC members strengthened with FRP materials. The majority of research studies dedicated to the analysis of the behaviour of continuous elements reports the use of the EBR technique. Limited information is available in the literature dealing with the behaviour of continuous structures strengthened according to the NSM technique. Thus, to contribute for a better understanding of the influence of the strengthening arrangement (hogging, sagging, or both regions) and percentage of FRP in terms of load carrying capacity, moment redistribution capacity, and ductility performance, an experimental program formed by continuous slab strips strengthened in flexure with near surface mounted (NSM) Carbon Fiber Reinforced Polymer (CFRP) laminates was carried out at the University of Minho (Bonaldo 2008; Dalfré 2013). The experimental program was composed of seventeen  $120 \times 375 \times 5875 \text{ mm}^3$  RC slab strips strengthened with NSM CFRP laminates, grouped in two series that are different in terms of strengthening configuration: H series, where H is the notation to identify the slabs strengthened with NSM CFRP laminates exclusively applied in the hogging region; HS series, where HS is the notation to identify the slabs strengthened with NSM CFRP laminates applied in both hogging and sagging regions. Figure 8.17 presents the test configuration adopted in the experimental program. The amount and disposition of the steel bars were designed to assure moment redistribution percentages ( $\eta$ ) of 15, 30 and 45 %. The NSM CFRP systems applied in the flexural strengthened RC slabs were designed to increase in 25 and 50 % the load carrying capacity of the reference slab. From the obtained results, it was verified that the strengthening configurations composed by laminates only applied in the hogging region did not attain the target increase of the load carrying capacity. When applying CFRP laminates in both sagging and hogging regions (HS series), the target increase of the load carrying capacity was attained. Therefore, to increase significantly the load carrying capacity of the RC slabs, the sagging zones need also to be strengthened. A moment redistribution percentage lower than the predicted one was determined in the slabs strengthened with CFRP laminates in the hogging region (H). For this strengthening configuration,  $\eta$  has decreased with the increase of the CFRP percentage. However, adopting a flexural strengthening strategy composed of CFRP laminates applied in both hogging and sagging regions, the target values for the moment redistribution capacity was attained and the influence of the percentage of CFRP on  $\eta$  was marginal.

#### *Simulation of RC slab strips strengthened with NSM CFRP laminates*

Numerical analyses were carried out to simulate the load-deflection relationship of concrete elements reinforced with conventional steel bars and strengthened by NSM CFRP laminate strips. For assessing the predictive performance of a FEM-based computer program, the experimental tests were simulated by considering the nonlinear relevant aspects of the intervening materials. In general, the numerical simulations have reproduced with high accuracy the behaviour of the carried out tests. Later, a parametric study composed of 144 numerical simulations

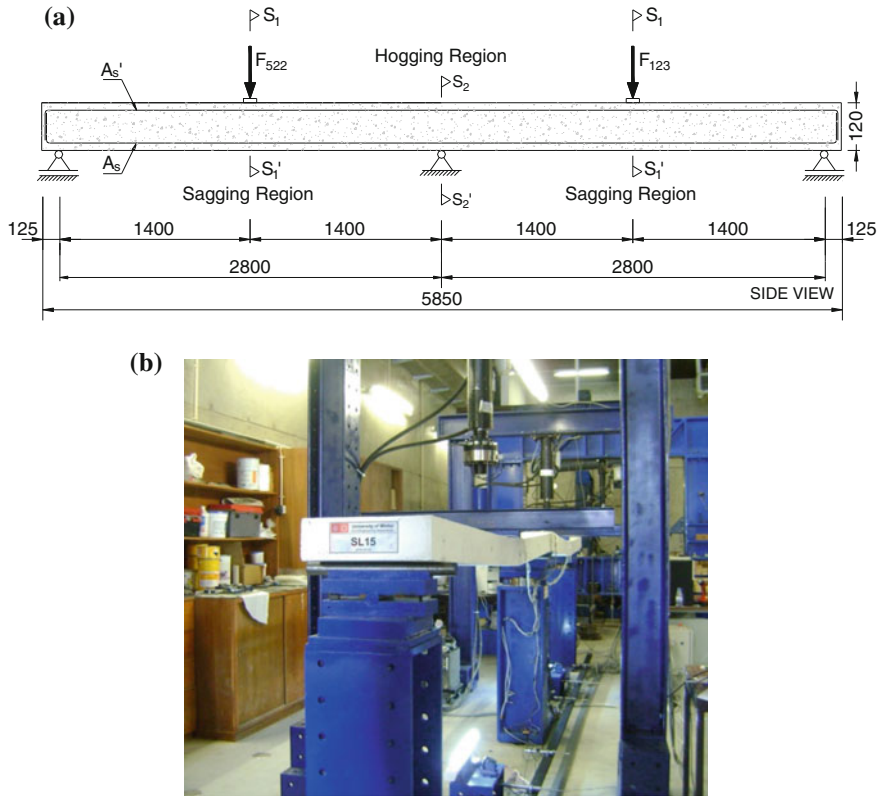


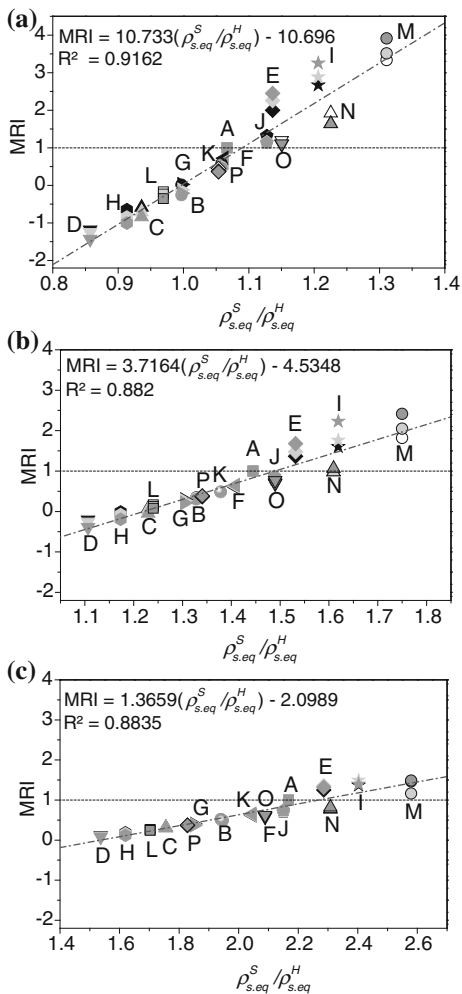
**Fig. 8.17** Test configuration for continuous RC slabs tests: **a** Scheme; **b** foto. Note: specimens dimensions are in mm

was carried out to investigate the influence of the strengthening arrangement and CFRP percentage in terms of load carrying capacity and moment redistribution capacity of continuous RC slab strips flexural strengthened by the NSM technique.

According to the results, the load carrying and the moment redistribution capacities strongly depend on the flexural strengthening arrangement. The load carrying capacity of the strengthened slabs increases with the equivalent reinforcement ratio  $[\rho_{s,eq} = A_s / (bd_s) + (A_f E_f / E_s) / (bd_f)]$  applied in the sagging and hogging regions ( $\rho_{s,eq}^S$  and  $\rho_{s,eq}^H$ , respectively), but the increase is much more pronounced with  $\rho_{s,eq}^S$ , specially up to the formation of the plastic hinge in the hogging region (Fig. 8.18).

The moment redistribution (*MRI*) is defined as the ratio between the  $\eta$  of a strengthened slab,  $\eta_{streng}$ , and the  $\eta$  of its reference slab,  $\eta_{ref}$ , ( $MRI = \eta_{streng} / \eta_{ref}$ ), where  $\eta$  is the moment redistribution percentage at the formation of the second hinge (in the sagging region). According to the results, the moment redistribution

**Fig. 8.18** Relationship between the moment redistribution index and  $\rho_{s,eq}^S/\rho_{s,eq}^H$  for series: **a** SL15, **b** SL30, and **c** SL45



has increased with  $\rho_{s,eq}^S/\rho_{s,eq}^H$  and positive values ( $MRI > 0$ , which means that the moment redistribution of the strengthened slab was higher than its corresponding reference slab) were obtained when  $\rho_{s,eq}^S/\rho_{s,eq}^H > 1.09$ ,  $\rho_{s,eq}^S/\rho_{s,eq}^H > 1.49$  and  $\rho_{s,eq}^S/\rho_{s,eq}^H > 2.27$  for  $\eta$  equal to 15, 30 and 45 %, respectively. Thus, the moment redistribution percentage can be estimated if  $\rho_{s,eq}^S/\rho_{s,eq}^H$  is known. Figure 8.19 presents the relationship between MRI and  $\rho_{s,eq}^S/\rho_{s,eq}^H$  for series SL15, SL30 and SL45. The results evidenced that the use of efficient strengthening strategies can provide adequate levels of ductility and moment redistribution in statically indeterminate structures, with a considerable increase in the load carrying capacity. Also, according to the results, a flexural strengthening strategy composed of CFRP

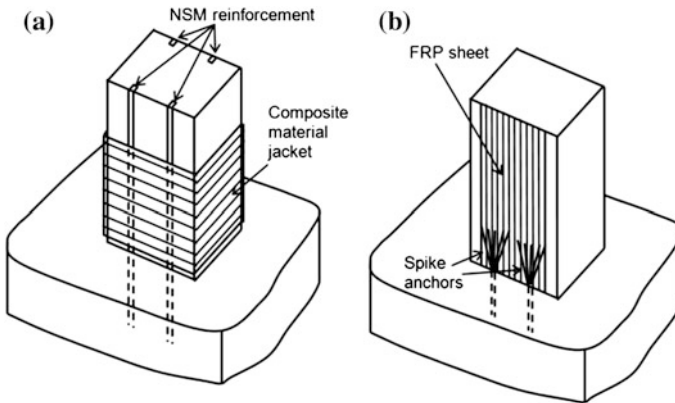


**Fig. 8.19** Flexural strengthening of RC column with: **a** NSM reinforcement combined with composite material jacketing; **b** externally bonded FRP sheets combined with spike anchors (possibly combined with jacketing, not shown for the sake of clarity)

laminates applied in both hogging and sagging regions has a deflection ductility performance similar to its corresponding RC slab.

Finally, the rotational capacity of the strengthened slab strips decreases with the increase of  $\rho_{s,eq}^H$ , and increases with  $\rho_{s,eq}^S$ . In the slab strips strengthened in both sagging and hogging regions, a rotational capacity lower than its reference slabs was obtained.

In conclusion, the obtained results evidence that the use of efficient strengthening strategies can provide adequate level of ductility and moment redistribution in statically indeterminate structures, with a considerable increase in the load carrying capacity.

## Columns

Flexural strengthening of RC columns is typically achieved today by using RC jackets or some forms of steel jackets, namely steel “cages”, also followed by shotcreting. RC jackets or steel cages covered by shotcrete require intensive labour and artful detailing, they increase the dimensions and weight of columns and result in substantial obstruction of occupancy. On the other hand, fibre reinforced polymer (FRP) jacketing, which addresses all of the above mentioned difficulties, is not applicable, as effective strengthening of columns in flexure calls for the continuation of externally applied longitudinal reinforcement beyond the end cross-sections, where moments are typically higher. To overcome the aforementioned difficulties and problems associated with conventional techniques and FRP jacketing, recent research efforts have focused on the use of innovative strengthening techniques:



flexural strengthening of RC columns may be achieved through the use of near-surface mounted (NSM) FRP (Alkhrdaji et al. 2001; Bournas and Triantafillou 2009; Perrone et al. 2009; Maaddawy and Dieb 2011) or through a combination of externally bonded (EBR) FRP sheets (or laminates) and anchors (Prota et al. 2005; Realfonzo and Napoli 2009; Vrettos et al. 2013). This form of externally applied longitudinal reinforcement is prevented from local buckling in highly compressed areas through the use of confining jackets made of composite materials with polymer-based (FRP) or inorganic matrices (textile-reinforced mortars—TRM (e.g. Bournas et al. 2007; Bournas and Triantafillou 2009; see Chap. 9)). These concepts are illustrated in Fig. 8.19.

### Test Specimens and Tests Setup

A number of experimental programs studied the flexural strengthening of old-type RC columns with NSM reinforcement (Alkhrdaji et al. 2001; Bournas and Triantafillou 2009; Perrone et al. 2009). In Bournas and Triantafillou (2009) and Perrone et al. (2009) large-scale RC columns were tested under cyclic uniaxial flexure with constant axial load (Fig. 8.20a). The specimens were flexure-dominated cantilevers, with a height to the point of application of the load of 1.6 or 1.5 m in Bournas and Triantafillou (2009) and Perrone et al. (2009), respectively, and a cross-section of  $250 \times 250 \text{ mm}^2$ . The geometry of a typical cross-section is shown in Fig. 8.20b. The specimens were designed such that the effect of a series of parameters on the flexural capacity of RC columns could be investigated. These parameters comprised: type of NSM reinforcement (CFRP strips, GFRP bars, stainless steel rebar); configuration of NSM reinforcement (CFRP strips placed with their large cross-section side perpendicular or parallel to the column sides, depending on whether a proper concrete cover is available or not); amount—that is geometrical reinforcing ratio—of NSM or internal reinforcement; type of bonding agent for the NSM reinforcement (epoxy resin vs. cement-based mortar); and NSM reinforcement with or without local jacketing at the member ends.

A short description of the specimens is given in Fig. 8.20c. Of crucial importance in the selection of NSM reinforcement was the requirement of equal tensile strength (not area or stiffness) for each of the reinforcing elements (CFRP strips, GFRP bars, stainless steel bars). The test setups adopted in Bournas and Triantafillou (2009) and Perrone et al. (2009) are identical with the columns fixed into a heavily reinforced base block, within which the longitudinal bars were anchored. The columns were subjected to lateral cyclic loading which consisted of successive cycles progressively increasing by 5 mm (or 2.5 mm in Perrone et al. 2009) of displacement amplitudes (0.31 % drift ratio) in each direction. At the same time a constant axial load was applied to the columns. The lateral load was applied using a horizontally positioned servo-hydraulic actuator. The axial load was exerted

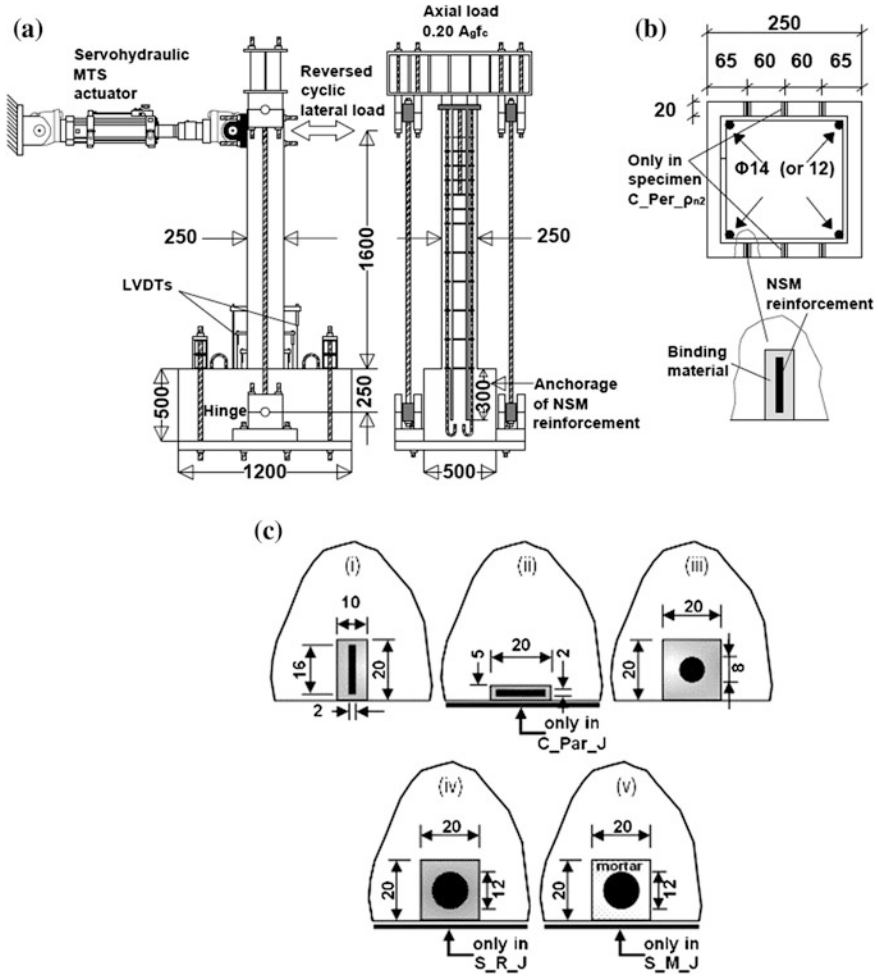


**Fig. 8.20** a Schematic of test setup. b Cross-section of columns. c Detail of NSM reinforcement configuration in columns: (i) C\_Per, C\_Per\_pn2, C\_Per\_ps2; (ii) C\_Par and C\_Par\_J; (iii) G; (iv) S\_R and S\_R\_J; and (v) S\_M and S\_M\_J. (dimensions in mm)

by a set of four hydraulic cylinders, acting against two vertical rods connected to the strong floor of the testing frame through a hinge (Fig. 8.20a). Displacements and axial strains at the plastic hinge region were monitored using LVDTs fixed at the cross sections close to the column base (Fig. 8.20a). The instrumentation also comprised a number of strain gages which were mounted on the NSM reinforcing elements to calculate the NSM reinforcement strain at failure.

## Failure Modes and Effective Strain

The flexural failure of RC columns strengthened in flexure with NSM reinforcement (FRP or stainless steel bars) occurs due to concrete crushing at the ultimate compressive strain,  $\varepsilon_c = \varepsilon_{ccu}$  (or  $\varepsilon_{cu}$  for unconfined concrete), or due to failure of the NSM reinforcement at a limiting strain  $\varepsilon_{n,lim}$ , which generally develops after yielding of the internal tension steel bars. This strain depends on the failure mode of the external reinforcement, which may be debonding or tensile rupture. For design purposes, the simplest approach to account for debonding is to calculate the strain in the external reinforcement at debonding,  $\varepsilon_{n,b}$ , as the product of the ultimate strain  $\varepsilon_{n,u}$  (the yield strain, in case of steel NSM reinforcement) and a bond reduction factor  $k_b$ . Debonding of the external reinforcement depends mainly on the anchorage length, configuration of rebar, nature of loading (monotonic or cyclic) and presence of external confinement. Experimental evidence (Bournas and Triantafillou 2009; Vrettos et al. 2013) suggests that even if failure of the external reinforcement is due to tensile rupture (in the case of FRP), the failure strain is, in general, less than the (monotonic) uniaxial ultimate strain derived from material testing. The effective ultimate tensile strain of FRP is calculated as the product of the ultimate tensile strain and an effectiveness reduction factor  $k_r$ , which depends mainly on the nature of loading (monotonic or cyclic) and the type of anchorage of the longitudinal reinforcement (e.g. configuration of spike anchors). Examples for the estimation of  $k_b$  and  $k_r$  may be found in Bournas and Triantafillou (2009) and Vrettos et al. (2013). As documented in these studies, if (a) flat FRP strips are used as NSM flexural reinforcement with their long side parallel to the column side, (b) the loading is cyclic, and (c) no confining jackets are used, then failure is due to debonding and  $k_b$  is about 0.25. If the same configuration is combined with jacketing, debonding is suppressed and failure is governed by rupture of the external reinforcement with  $k_r$  about 0.67. If the strips are used with their long side perpendicular to the column side (without confining jacket) failure is governed by rupture with  $k_r$  of about 0.5. If the NSM FRP is in the form of rebars with circular section, failure is controlled by debonding with  $k_b$  about 0.35. If FRP spike anchors are used with sufficient anchorage length so that failure is controlled by rupture (Vrettos et al. 2013), the effective strength of those anchors (in the case of cyclic loading) is approximately equal to 30 % of the tensile strength of straight fibres, hence  $k_r = 0.30$ . Finally, if the NSM reinforcement comprises properly anchored stainless steel rebar, those rebar yield prior to failure of the cross section due to concrete crushing, hence  $k_r = 1$ . All values for  $k_b$  and  $k_r$  given above should be considered as indicative, as they have been derived on the basis of relatively limited test results. The point to be made here is that, if the cross-section failure mode involves failure of the NSM flexural reinforcement, the cross-section analysis can be made with the strain in the external reinforcement equal to a (known) fraction of the ultimate uniaxial tension strain, to be determined through testing.

### Load-Deflection Response

The response of the columns tested in Bournas and Triantafillou (2009) and Perrone et al. (2009) is given in Fig. 8.21 in the form of load-drift ratio and load-deflection loops, respectively. In Bournas and Triantafillou (2009) the control specimen attained a peak load of about 33 kN and a drift ratio at failure of 6.25 %. With only one exception (column C\_Par) all strengthened specimens displayed considerably higher (from about 25 % up to about 100 %) flexural resistance compared to the control specimen.

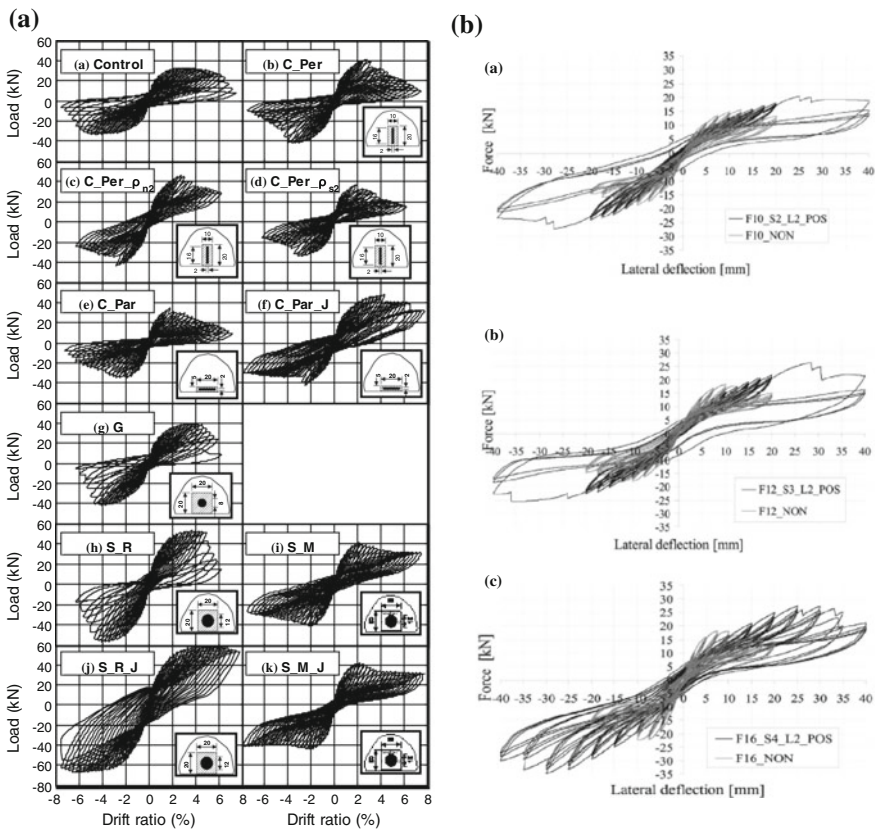


**Fig. 8.21** a Load versus drift ratio curves for tested specimens in Bournas and Triantafillou (2009); b Load versus displacement curves for tested specimens in Perrone et al. (2009)

## Influence of Different Parameters on the Flexural Strengthening Performance

*Type of NSM reinforcement (C\_Per vs. G vs. S\_R).* Despite the roughly equal (monotonic) uniaxial strength of CFRP, GFRP and stainless steel bars, the latter were more effective, resulting in a strength increase equal to 64 %. The respective values for FRPs were lower (26 % for CFRP and 22 % for GFRP), due to failure of the FRP reinforcing elements at strains less than those corresponding to peak stress, as a result of cyclic loading. In terms of deformation capacity, quantified here by the drift ratio at conventional failure, stainless steel and GFRP bars outperformed CFRP strips by approximately 25 %, due to the lower deformability of carbon fibres in comparison with the other two materials.

*Geometrical reinforcing ratio of NSM reinforcement (C\_Per vs. C\_Per\_ρ<sub>n2</sub>).* Increasing the NSM reinforcing ratio by 50 % (three vs. two strips in each side) resulted in a nearly proportional increase in column's strength, which is from 26 % in specimen C\_Per to 35 % in specimen C\_Per\_ρ<sub>n2</sub>. This linearity may not apply in the case of large NSM reinforcing ratios.

*Configuration of NSM strips (C\_Per versus C\_Par).* In the absence of local jacketing, NSM strips placed with their larger cross-section side perpendicular to the column side were far more effective than those with their larger cross section side parallel to the column side, due to the more favourable bond conditions. The strength increase in the former case was 26 %, but only 4 %, that is marginal, in the latter case.

*NSM reinforcement with or without local jacketing (C\_Par versus C\_Par\_J, S\_R versus S\_R\_J, S\_M versus S\_M\_J).* TRM jackets resulted in dramatic improvements of the retrofitted specimens' response, by increasing both strength and deformation capacity. Jacketing with TRM prevented buckling of the NSM reinforcement, thereby making the strength increase from 4 to 36 % in the case of CFRP and from 64 to 90 % in the case of stainless steel. In columns retrofitted with NSM bars placed inside mortar, jacketing offered a marginal increase in strength and a moderate increase in deformation capacity. Of all NSM systems examined, the one comprising stainless steel bars and TRM jacketing displayed the best response with stable post peak behaviour and minimal strength degradation up to large drift ratios. NSM FRP or stainless steel reinforcement is a viable solution towards enhancing the flexural resistance of reinforced concrete columns subjected to seismic loads. With proper design, which should combine compulsory NSM reinforcement with local jacketing at column ends, it seems that column strength enhancement does not develop at the expense of low deformation capacity.

*Type of bonding agent (S\_R versus S\_M, S\_R\_J versus S\_M\_J).* Epoxy resin was a much more effective bonding agent for NSM stainless steel. For the unjacketed specimens, when mortar was used (S\_M) instead of resin (S\_R) the increase in strength dropped from 64 to 24 %; the corresponding values for jacketed specimens were 90 and 29 %. Hence, the use of mortar instead of resin reduced the effectiveness of the strengthening scheme to about 1/3, due to pullout of the NSM bars.

### Design of NSM Strengthened Columns Subjected to Biaxial Bending

Numerical and analytical modelling of columns strengthened with the NSM technique was implemented in Barros et al. (2008) and Bournas and Triantafillou (2013), respectively. Cyclic material constitutive laws were implemented in a finite element program and the tests with RC columns strengthened with the NSM technique were numerically simulated under cyclic loading in Barros et al. (2008). These numerical simulations reproduce the experimental load displacement diagrams satisfactorily. The modelling of the biaxial bending in columns strengthened with NSM reinforcement in combination with confinement proposed in Bournas and Triantafillou (2013) is presented. For any rectangular cross-section subjected to biaxial bending with axial force, the neutral axis is inclined, as shown in Fig. 8.22. The corresponding slope depends on the ratio of the bending moments in the two orthogonal directions and the mechanical properties of the cross-section. Some details of the cross-section analysis are given next.

The strains in the internal reinforcement,  $\epsilon_{si}$  ( $i = 1, 2, 3, 4$ ), and in the external reinforcement,  $\epsilon_{nib}$  and  $\epsilon_{nih}$  ( $i = 1, 2, 3, 4$ ), may be found from similar triangle in terms of the strain at the extreme concrete fibre,  $\epsilon_c$ , and the geometrical quantities  $x$ ,  $h$ ,  $b$ ,  $d_s$ ,  $b_s$ ,  $d_b$ ,  $b_b$ ,  $d_h$ ,  $b_h$ , and  $\theta$  (angle of the neutral axis with respect to side  $h$ ), all defined in Fig. 8.22. To account for internal steel yielding, failure of the external reinforcement (debonding or fracture in case of FRP, yielding in case of stainless steel) or concrete crushing, strain compatibility should be checked. For the case of external FRP the conditions to be checked are the following:

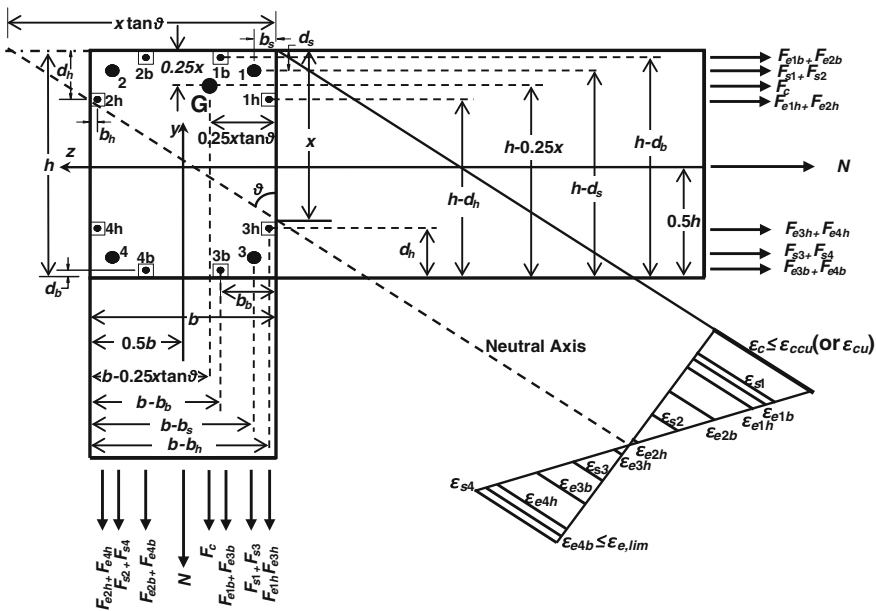


Fig. 8.22 Internal forces and strains at cross section subjected to biaxial bending with axial force

$$\text{If } \varepsilon_{si} \geq \frac{f_y}{E_s} \quad \text{then } f_{si} = f_y \quad (8.5a)$$

$$\text{If } \frac{f_y}{E_s} > \varepsilon_{si} > -\frac{f_y}{E_s} \quad \text{then } f_{si} = E_s \cdot \varepsilon_{si} \quad (8.5b)$$

$$\text{If } \varepsilon_{si} \leq -\frac{f_y}{E_s} \quad \text{then } f_{si} = -f_y \quad (8.5c)$$

$$\max(\varepsilon_{e4b}, \varepsilon_{e4h}) \leq \varepsilon_{e,lim} \quad (8.6)$$

$$\varepsilon_c \leq \varepsilon_{ccu} \text{ for confined concrete or } \varepsilon_{cu} \text{ for unconfined} \quad (8.7)$$

$$\text{If } \varepsilon_{si} \geq \frac{f_y}{E_s} \quad \text{then } f_{si} = f_y \quad (8.8a)$$

$$\text{If } \frac{f_y}{E_s} > \varepsilon_{si} > -\frac{f_y}{E_s} \quad \text{then } f_{si} = E_s \cdot \varepsilon_{si} \quad (8.8b)$$

$$\text{If } \varepsilon_{si} \leq -\frac{f_y}{E_s} \quad \text{then } f_{si} = -f_y \quad (8.8c)$$

$$\max(\varepsilon_{e4b}, \varepsilon_{e4h}) \leq \varepsilon_{e,lim} \quad (8.9)$$

$$\varepsilon_c \leq \varepsilon_{ccu} \text{ for confined concrete or } \varepsilon_{cu} \text{ for unconfined} \quad (8.10)$$

The forces of internal steel bars and external reinforcement can be computed as follows:

$$F_{si} = A_{si} \cdot f_{si} \quad (8.11)$$

$$F_{eib} = A_{eib} \cdot E_e \cdot \varepsilon_{eib} \quad (8.12)$$

$$F_{eih} = A_{eih} \cdot E_e \cdot \varepsilon_{eih} \quad (8.13)$$

where  $A_{si} = A_s/4$  = area of internal steel reinforcement concentrated at section's corners,  $A_{nib} = A_{nb}/4$  = area of NSM reinforcement lumped at each position on side  $b$ ,  $A_{nih} = A_{nh}/4$  = area of external reinforcement lumped at each position on side  $h$  and  $E_n$  = elastic modulus of NSM reinforcement. For concrete in the "elastic" range (stresses less than  $f_{co}$ ) the magnitude of concrete's compressive stress resultant  $F_c$  is equal to the volume of a triangular pyramidal stress block (OABC in Fig. 8.23) with a height taken to be the maximum stress of concrete at a corner point. For concrete strains above  $\varepsilon_{co}$  the material behaves nonlinearly and the compression stress block (OABGDE in Fig. 8.23) becomes complex. The complexity of the analysis in this case can be reduced and the nonlinear stress calculations can be reduced to a sequence of linear ones, by computing the volume

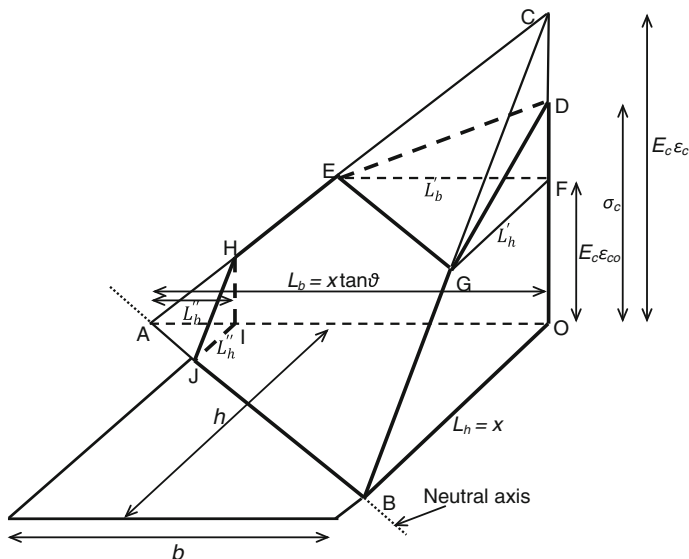


Fig. 8.23 Pyramidal compressive stress block in concrete

of the nonlinear stress block (that is the compressive stress resultant) as the algebraic sum of volumes of simple triangular pyramidal stress blocks as follows:

$$F_c = V_{OABC} - V_{FEGC} + V_{FEGD} - V_{AIJH} \tag{8.14}$$

Hence:

$$F_c = \frac{1}{6} L_h L_b E_c \epsilon_c - \frac{1}{6} L'_h L'_b E_c (\epsilon_c - \epsilon_{co}) + \frac{1}{6} L'_h L''_b \frac{(f_{cc} - f_{co})}{(\epsilon_{ccu} - \epsilon_{co})} - \frac{1}{6} L''_h L''_b E_c \left( \epsilon_c \frac{L''_b}{L_b} \right) \tag{8.15}$$

where  $L_h = x =$  neutral axis depth parallel to side  $h$  (Fig. 8.23),  $L_b = x \tan \theta =$  neutral axis depth parallel to side  $b$ ,  $E_c =$  elastic modulus of concrete and  $L'_h, L'_b, L''_h, L''_b$  as given by the following relationships (Fig. 8.23):

$$L'_h = \frac{(\epsilon_c - \epsilon_{co})}{\epsilon_c} L_x, \quad L'_b = \frac{(\epsilon_c - \epsilon_{co})}{\epsilon_c} L_b, \quad L''_h = L_h - b \tan \theta, \quad L''_b = L_h - b \tag{8.16}$$

The equations presented above have three unknown quantities:  $x$  and  $\tan \theta$ , which define the position of the neutral axis, as well as  $\epsilon_c$  that is the maximum compressive strain in the concrete. These unknowns can be determined through the use of axial force and moment equilibrium:



$$N = F_c + \sum_{i=1}^4 F_{si} + \sum_{i=1}^4 F_{eib} + \sum_{i=1}^4 F_{eih} \quad (8.17)$$

$$\begin{aligned} M_y = & F_c \left( \frac{b}{2} - 0.25 \cdot x \cdot t g \theta \right) + (F_{s1} - F_{s2} + F_{s3} - F_{s4}) \left( \frac{b}{2} - b_s \right) \\ & + (F_{e1b} - F_{e2b} + F_{e3b} - F_{e4b}) \left( \frac{b}{2} - b_b \right) \\ & + (F_{e1h} - F_{e2h} + F_{e3h} - F_{e4h}) \left( \frac{b}{2} - b_h \right) \end{aligned} \quad (8.18)$$

$$\begin{aligned} M_z = & F_c \left( \frac{b}{2} - 0.25 \cdot x \right) + (F_{s1} + F_{s2} - F_{s3} - F_{s4}) \left( \frac{h}{2} - d_s \right) \\ & + (F_{e1b} + F_{e2b} - F_{e3b} - F_{e4b}) \left( \frac{h}{2} - d_b \right) \\ & + (F_{e1h} + F_{e2h} - F_{e3h} - F_{e4h}) \left( \frac{h}{2} - d_h \right) \end{aligned} \quad (8.19)$$

where  $N$  is the (compressive) axial force in the column and  $M_y$  and  $M_z$  are the bending moments with respect to the two centroidal axes  $y$  and  $z$ , respectively (Fig. 8.22). To account for the effect of possible confinement provided by composite material jacketing, the compressive stress–strain response of concrete is modelled as bilinear, in agreement with extensive experimental evidence. According to the typical approach toward modelling confinement of concrete by composite materials, the confined strength  $f_{cu}$  and ultimate strain  $\varepsilon_{ccu}$ , depend on the confining stress at failure (fracture of the jacket in the circumferential direction),  $\sigma_{lu}$ , as follows (Bournas and Triantafillou 2013):

$$\frac{f_{cc}}{f_{co}} = 1 + k_1 \left( \frac{\sigma_{lu}}{f_{co}} \right)^m \quad (8.20)$$

$$\frac{\varepsilon_{ccu}}{\varepsilon_{co}} = 1 + k_2 \left( \frac{\sigma_{lu}}{f_{co}} \right)^n \quad (8.21)$$

The confining stress  $\sigma_l$  is, in general, non-uniform, especially near the corners of rectangular cross sections. As an average for  $\sigma_l$  in a cross section with dimensions  $b$  and  $h$  one may write (Bournas and Triantafillou 2013):

$$\sigma_l = \frac{\sigma_{lh} + \sigma_{lb}}{2} = \frac{1}{2} \alpha_f \left( \frac{2t_j}{h} E_j \varepsilon_j + \frac{2t_j}{h} E_j \varepsilon_j \right) \quad (8.22)$$

where  $E_j$  and  $\varepsilon_j$  are the elastic modulus and strain, respectively, of the composite material jacket in the circumferential direction,  $t_j$  is the jacket thickness and  $\alpha_f$  is a

confinement effectiveness coefficient, which is defined as the ratio of effectively confined area  $A_e$  to the total cross-sectional area  $A_g$  as follows (fib 2001):

$$\alpha_f = 1 - \frac{(b - 2r_c)^2 + (h - 2r_c)^2}{3bh} \quad (8.23)$$

Hence, the confining stress at failure,  $\sigma_{lu}$ , is given by Eq. (8.24) with  $E_j \varepsilon_j$  replaced by  $f_{je}$ , the effective jacket strength in the circumferential direction. Finally, the normalized confining stress at failure is written as:

$$\frac{\sigma_{lu}}{f_{co}} = \frac{\sigma_{luh} + \sigma_{lub}}{2f_{co}} = \frac{1}{2} \alpha_f \left( \frac{2t_j f_{je}}{h f_{co}} + \frac{2t_j f_{je}}{b f_{co}} \right) = \frac{1}{2} \alpha_f (\omega_{fh} + \omega_{fb}) \quad (8.24)$$

where  $\omega_{fh} = (2t_j/h)(f_{je}/f_{co})$  and  $\omega_{fb} = (2t_j/b)(f_{je}/f_{co})$  are the mechanical ratios of composite confining jacket in the direction perpendicular to side  $h$  and  $b$ , respectively. The literature on the precise form of confinement models for concrete, that is, on values for the empirical constants in Eqs. (8.20) and (8.21), is vast. In this study it was assumed that  $k_1 = 2.6$ ,  $m = 2/3$ ,  $k_2 = 7.5$ , and  $n = 0.5$ . However, the confinement model may be used with any other set of data for those empirical constants.

### Comparison of the Analytical and Numerical Models with Test Results

The analytical procedure described was implemented in a computer program (Bournas and Triantafillou 2013). The program uses geometrical and material data as input to yield, through an iterative numerical procedure, bending moment—axial force interaction diagrams for different cross-sections. This computer program was used to facilitate the comparison of analytical predictions with test results identified in the literature on flexural strengthening of RC columns with NSM reinforcement. Such results are limited and apply mainly to the case of uniaxial or biaxial bending with axial force in columns strengthened with NSM rebar (Alkhrdaji et al. 2001; Bournas and Triantafillou 2009; Perrone et al. 2009; Maaddawy and Dieb 2011), whereas a few test results may be found for the case of uniaxial bending with axial force in columns with anchors or anchorage devices (fibre-based or metallic) at the critical cross-sections (Prota et al. 2005; Realfonzo and Napoli 2009; Vrettos et al. 2013). These results are summarized in Fig. 8.24a, where the predicted to experimental moment ratio is plotted for each column. The mean and the standard deviation of the ratio of the predicted-to-experimental value of normalized ultimate moments  $\mu_{max}$  are equal to 0.985 and 0.111, respectively. The overall agreement between analysis and test results is quite satisfactory. Finally, it should be mentioned that the numerical model developed in Barros et al. (2008) reproduced with good agreement the load-deflection response of NSM strengthened columns as illustrated in Fig. 8.24b.

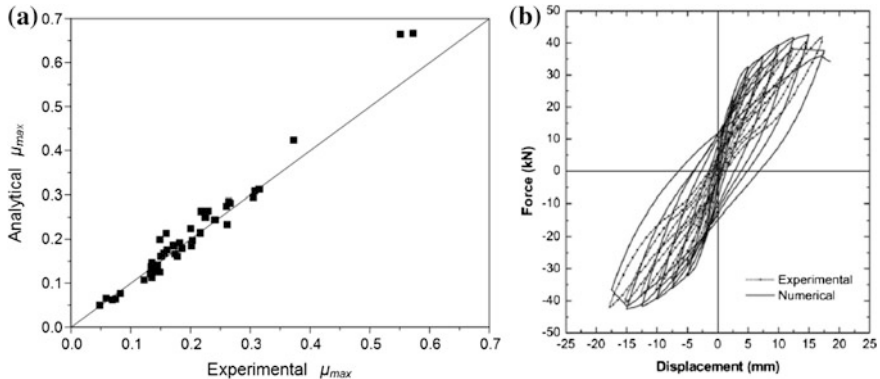


**Fig. 8.24** **a** Comparison of experimental normalized bending moment capacity with value predicted by analytical model proposed in Bournas and Triantafillou (2013). **b** Comparison of experimental force-displacement response of an NSM strengthened column with the numerical model developed in Barros et al. (2008)

## Shear Strengthening

Experimental research has demonstrated that the near surface mounted technique (NSM) is very effective for the shear strengthening of reinforced concrete (RC) beams (Barros and Dias 2006; Kotynia 2007b; El-Hacha and Wagner 2009). Available experimental results evidence that FRP reinforcements of rectangular cross section provide the greater shear strengthening effectiveness, due to larger ratio between the FRP-concrete bond perimeter and the cross sectional area of the FRP reinforcement, as well as larger confinement provided by the surrounding concrete to the FRP (Costa and Barros 2011). The FRP reinforcements are positioned orthogonally to the beam's axis, or as orthogonal as possible to the predicted direction of the shear failure crack, or to the already existing shear cracks. Carbon FRP (CFRP) laminates of rectangular cross section have been the most used in the NSM technique, so the design formulations herein proposed were mainly developed and calibrated by using experimental results from tests executed with RC beams shear strengthened with CFRP laminates, but their good predictive performance was also demonstrated when applied to other types of NSM FRP shear reinforcements.

The available experimental research also demonstrates that the NSM shear strengthening effectiveness is mainly dependent on the following parameters: percentage and orientation of the FRP reinforcements, concrete strength, and percentage of existing steel stirrups. The strengthening intervention often involves concrete elements already cracked. However, the experimental tests show that the main difference of the behaviour of NSM FRP beams with and without pre-cracks resides in an expected loss of initial stiffness in the pre-cracked beams (Dias and Barros 2012). In these beams the mobilization of the FRP reinforcements started

just after the opening process of the pre-cracks, while the mobilization of the FRP reinforcements in the non-pre-cracked beams only occurred when the shear crack has formed. However, the pre-cracking did not affect the efficacy of the NSM shear strengthening technique in terms of load carrying capacity and ultimate deflection.

## ***Design Approaches***

Two design approaches are proposed in this chapter. One is supported on extensive experimental program (Dias 2008), whose relevant results are resumed elsewhere (Dias and Barros 2013). The second one (Bianco et al. 2013) is a simplification of a more general formulation based on an original interpretation of the NSM shear strengthening phenomena for RC beams that fulfils equilibrium, kinematic compatibility, and constitutive law of both the adhered materials and the bond between them (Bianco et al. 2010). The former approach is herein designated as “Experimental-base model”, while the latter is named “Physical-mechanical-base model”.

### **Experimental-Base Model**

According to this model the force resulting from the tensile stress in the FRP laminates crossing the shear failure crack ( $F_f$ ) is defined as,

$$F_f = n_f \cdot A_{fv} \cdot f_{fe} \quad (8.25)$$

where  $f_{fe}$  is the effective stress in the laminates, which is obtained multiplying the elastic modulus of the FRP,  $E_f$ , by the effective strain,  $\varepsilon_{fe}$ . In Eq. (8.25)  $A_{fv}$  is the cross-sectional area of a FRP shear reinforcement that is formed by two lateral elements:

$$A_{fv} = 2 \cdot a_f \cdot b_f \quad (8.26)$$

where  $a_f$  and  $b_f$  are the dimensions of the reinforcement cross-section. The number of reinforcements crossed by the shear failure crack ( $n_f$ ) is obtained by the equation:

$$n_f = \frac{h_w \cdot (\cotg \alpha + \cotg \theta_f)}{s_f} \quad (8.27)$$

where (Fig. 8.25)  $h_w$  is the web depth of the beam (equal to the length of vertical reinforcements),  $\alpha$  is the orientation of the shear failure crack,  $\theta_f$  is the inclination of the FRP reinforcement with respect to the beam axis, and  $s_f$  is the spacing of laminates.

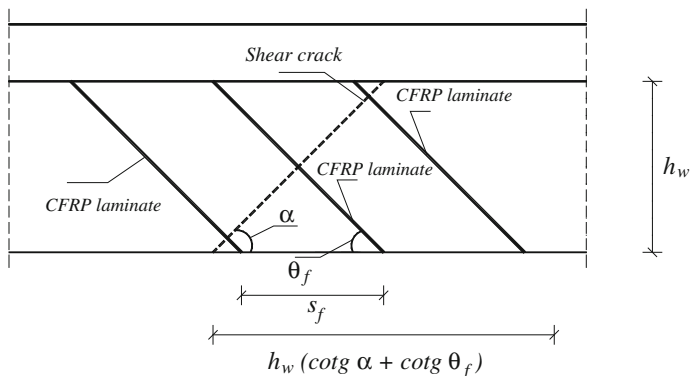


**Fig. 8.25** Data for the analytical definition of the effective strain of the FRP

The vertical projection of the force  $F_f$  is the contribution of the FRP to the shear resistance of the beam ( $V_f$ ):

$$V_f = F_f \cdot \sin \theta_f \tag{8.28}$$

Considering Eqs. (8.25)–(8.28) the value of  $V_f$  can be obtained from:

$$V_f = h_w \cdot \frac{A_{fv}}{s_f} \cdot \varepsilon_{fe} \cdot E_f \cdot (\cotg \alpha + \cotg \theta_f) \cdot \sin \theta_f \tag{8.29}$$

and, consequently:

$$\varepsilon_{fe} = V_f / \left( h_w \cdot \frac{A_{fv}}{s_f} \cdot E_f \cdot (\cotg \alpha + \cotg \theta_f) \cdot \sin \theta_f \right) \tag{8.30}$$

Based on the data derived from the experimental programs described in Dias (2008) and Dias and Barros (2013) the equation to obtain the value of the parameter  $\varepsilon_{fe}$  for the possible distinct NSM shear strengthening configurations is the following one:

$$\varepsilon_{fe} = 3.76888 \cdot e^{(-0.1160261 \theta_f + 0.0010437 \theta_f^2)} \cdot \left[ (E_f \rho_f + E_s \rho_{sw}) / (f_{cm}^{2/3}) \right]^{-0.460679} \cdot e^{(0.0351199 \theta_f - 0.0003431 \theta_f^2)} \tag{8.31}$$

where  $f_{cm}$  is the average concrete compressive strength,  $\rho_f = ((2 \cdot a_f \cdot b_f) / (b_w \cdot s_f \cdot \sin \theta_f))$  is the percentage of FRP shear reinforcement, and  $E_s$  and  $\rho_{sw} = (A_{sw} / (b_w \cdot s_w))$  are the elastic modulus and the percentage of existing steel stirrups, respectively.

**Fig. 8.26** Comparison between the experimental and analytical values of the CFRP contribution for the shear resistance ( $V_f$ )

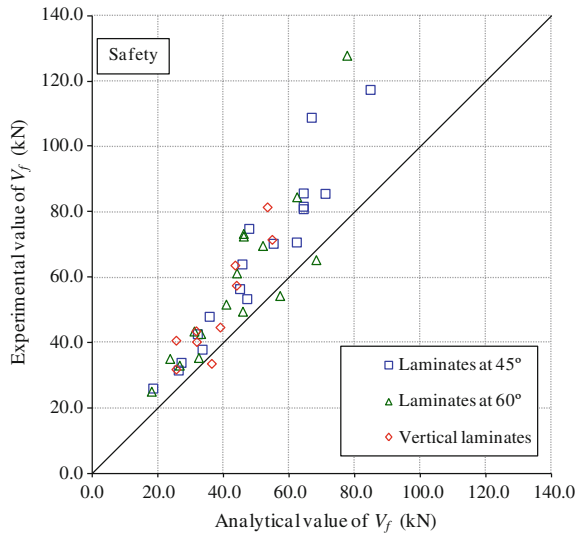
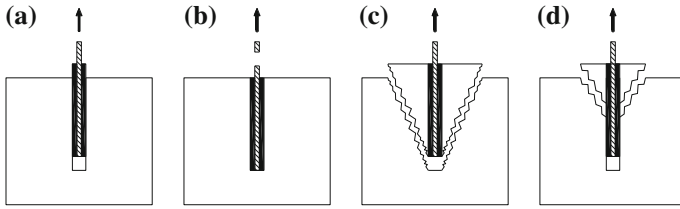


Figure 8.26 compares the experimental and the analytical values of  $V_f$  ( $V_f^{\text{exp}}$  and  $V_f^{\text{ana}}$ , respectively) for the beams considered in the development of the analytical formulation (Dias 2008; Dias and Barros 2013). According to this figures 95 % of the considered beams are in the safety zone (at the left side of diagonal line). Furthermore, the average value of the  $k$  parameter ( $k = V_f^{\text{exp}} / V_f^{\text{ana}}$ ) considering the safety factor  $\gamma_f$  equal to 1.3 was 1.31, and the corresponding standard deviation value was 0.18.

### Physical-Mechanical-Base Model

The physical-mechanical-base model assumes that the possible failure modes that can affect the ultimate behaviour of a NSM FRP reinforcement comprise: loss of bond (debonding); concrete semi-pyramidal tensile fracture; mixed shallow-semi-pyramid-plus-debonding and FRP tensile rupture (Fig. 8.27). This follows from the successive simplifications of the original model (Bianco et al. 2010) in order to result a closed form approach suitable for design purposes (Bianco et al. 2013).

The input parameters of this model include (Figs. 8.28 and 8.29) (Bianco et al. 2013): beam cross-section web's depth  $h_w$  and width  $b_w$ ; inclination angle of both CDC and FRP with respect to the beam longitudinal axis,  $\theta$  and  $\beta$ , respectively; FRP spacing measured along the beam axis,  $s_f$ ; angle  $\alpha$  between axis and principal generatrices of the semi-pyramidal fracture surface (Fig. 8.28c–d); concrete average compressive strength,  $f_{cm}$ ; FRP tensile strength,  $f_{fu}$ , and Young's modulus  $E_f$ ; thickness,  $a_f$ , and width,  $b_f$ , of the FRP cross-section, and values of bond stress,  $\tau_0$ , and slip,  $\delta_1$ , defining the adopted local bond stress-slip relationship (Fig. 8.28b).



**Fig. 8.27** Possible failure modes of an NSM FRP strip: **a** Debonding, **b** FRP tensile rupture, **c** concrete semi pyramidal fracture, **d** mixed shallow semi pyramid plus debonding

The implementation of the proposed calculation procedure comprehends the following steps (Fig. 8.29) (Bianco et al. 2013): (1) evaluation of the average value of the available (resisting) bond length  $\bar{L}_{Rfi}$  (Eq. 8.32) and of the minimum integer number  $N_{f,int}^l$  of NSM reinforcements that can effectively cross the CDC (Eq. 8.33); (2) evaluation of various constants, both integration and geometric ones (Eqs. 8.34–8.39); (3) evaluation of the bond-modeling constants (Eqs. 8.40 and 8.41); (4) evaluation of the reduction factor  $\eta$  of the average value of the available (resisting) bond length (Eqs. 8.42–8.44) and of the equivalent value of the average resisting bond length  $\bar{L}_{Rfi}^{eq}$  (Eq. 8.45); (5) evaluation of the value of the imposed end slip  $\delta_{Lu}$  in correspondence of which the peak value of the force transmissible through bond by the equivalent value of the resisting bond length  $\bar{L}_{Rfi}^{eq}$  can be attained (Eqs. 8.46–8.48); (6) evaluation of the maximum effective capacity that a NSM of bond length  $\bar{L}_{Rfi}^{eq}$  can attain during the beam loading process ( $V_{fi,eff}^{max}$ ) (Eqs. 8.49 and 8.50); (7) evaluation of the FRPs shear strength contribution  $V_f$  (Eq. 8.51).

$$\bar{L}_{Rfi} = \frac{h_w \cdot \sin \theta \cdot (\cot \theta + \cot \beta)}{4 \cdot \sin(\theta + \beta)} \quad (8.32)$$

$$N_{f,int}^l = \text{round off} \left[ h_w \cdot \frac{(\cot \theta + \cot \beta)}{s_f} \right] \quad (8.33)$$

$$L_p = 2 \cdot b_f + a_f \quad (8.34)$$

$$A_c = s_f \cdot \frac{b_w}{2} \quad (8.35)$$

$$L_d = \frac{h_w}{\sin \theta} \quad (8.36)$$

$$V_f^r = a_f \cdot b_f \cdot f_{fu} \quad (8.37)$$

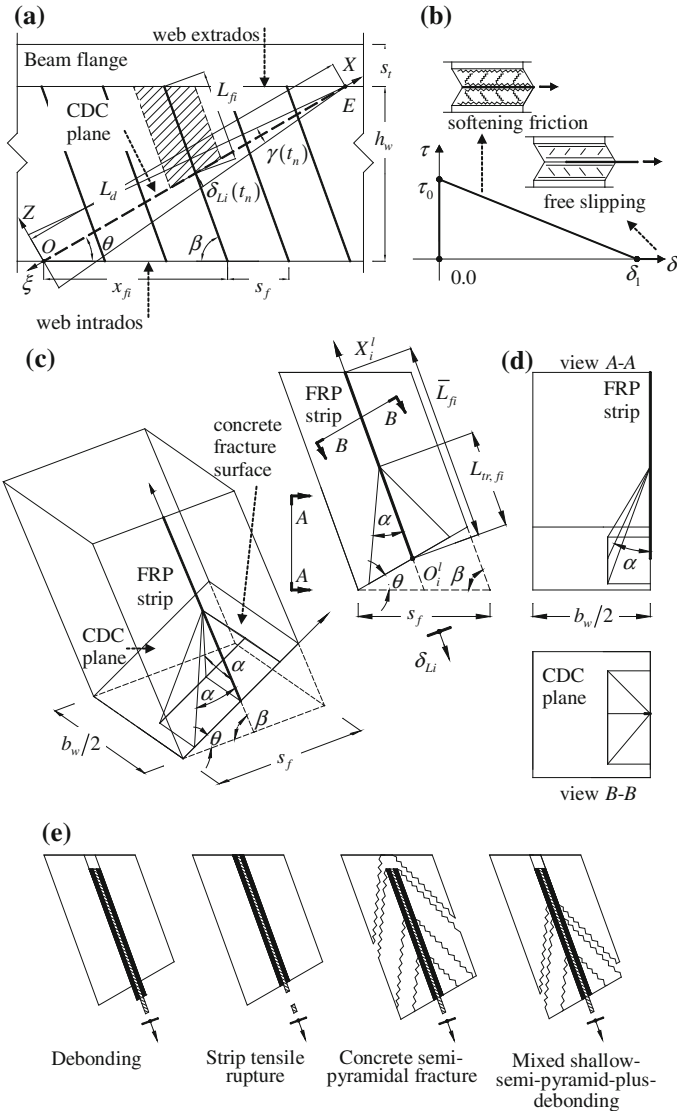


**Fig. 8.28** Main physical mechanical features of the theoretical model and calculation procedure: **a** Average available bond length of the NSM reinforcement and concrete prism of influence, **b** adopted local bond stress slip relationship, **c** NSM reinforcement confined to the corresponding concrete prism of influence and semi pyramidal fracture surface, **d** sections of the concrete prism (Bianco et al. 2013)



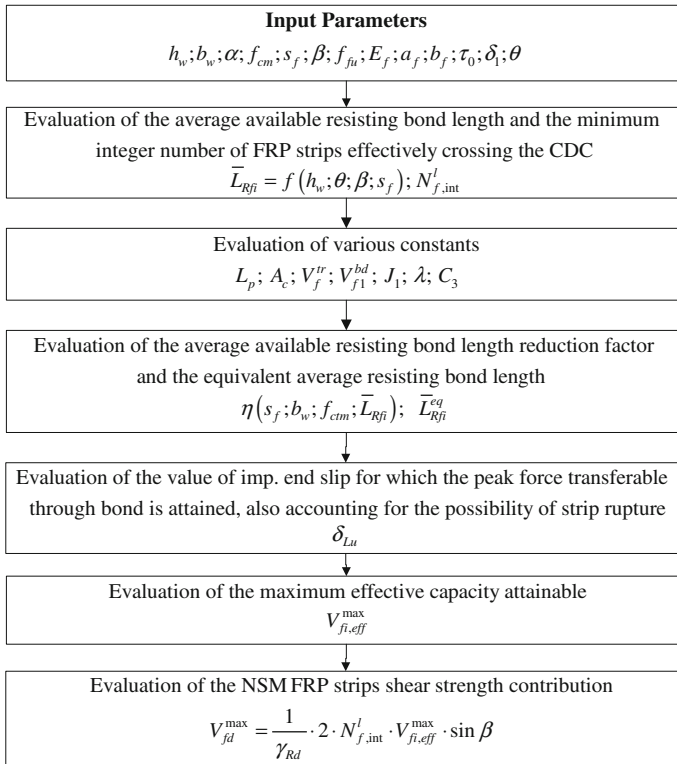


Fig. 8.29 Main algorithm of the calculation procedure (Bianco et al. 2013)

$$f_{ctm} = 1.4 \cdot ((f_{cm} - 8)/10)^{\frac{2}{3}} \tag{8.38}$$

$$E_c = 2.15 \cdot 10000 \cdot (f_{cm}/10)^{\frac{1}{3}} \tag{8.39}$$

$$J_1 = \frac{L_p}{A_f} \cdot \left[ \frac{1}{E_f} + \frac{A_f}{A_c \cdot E_c} \right] \quad \frac{1}{\lambda^2} = \frac{\delta_1}{\tau_0 \cdot J_1} \quad C_3 = \frac{V_f^{ir} \cdot J_1}{L_p \cdot \lambda} \tag{8.40}$$

$$L_{Rfe} = \frac{\pi}{2 \cdot \lambda}; \quad V_{f1}^{bd} = \frac{L_p \cdot \lambda \cdot \delta_1}{J_1} \tag{8.41}$$

$$\eta(s_f; b_w; f_{cm}; \bar{L}_{Rfi}) = \begin{cases} f_{ctm}/f_{ctm}^* & \text{se } f_{ctm} < f_{ctm}^* \\ 1 & \text{se } f_{ctm} \geq f_{ctm}^* \end{cases} \tag{8.42}$$

$$f_{ctm}^* = \frac{L_p \cdot \lambda \cdot \delta_1 \cdot \sin(\lambda \cdot L_{Rfi})}{J_1 \cdot \min(L_{Rfi} \cdot \tan \alpha; \frac{b_w}{2}) \cdot \min(s_f \cdot \sin \beta; 2 \cdot L_{Rfi} \cdot \tan \alpha)} \tag{8.43}$$

$$L_{Rfi} = \begin{cases} \bar{L}_{Rfi} & \text{if } \bar{L}_{Rfi} \leq L_{Rfe} \\ L_{Rfe} & \text{if } \bar{L}_{Rfi} > L_{Rfe} \end{cases} \quad (8.44)$$

$$\bar{L}_{Rfi}^{eq} = \bar{L}_{Rfi} \cdot \eta(s_f; b_w; f_{cm}; \bar{L}_{Rfi}) \quad (8.45)$$

$$\delta_{Lu} = \begin{cases} \delta_{L1}(\bar{L}_{Rfi}^{eq}) & \text{if } V_{f1}^{bd} < V_f^{tr} \\ \min[\delta_{L1}(\bar{L}_{Rfi}^{eq}); \delta_{Li}(V_f^{tr})] & \text{if } V_{f1}^{bd} \geq V_f^{tr} \end{cases} \quad (8.46)$$

$$\delta_{L1}(\bar{L}_{Rfi}^{eq}) = \begin{cases} \delta_1 \cdot [1 - \cos(\lambda \cdot \bar{L}_{Rfi}^{eq})] & \text{for } \bar{L}_{Rfi}^{eq} \leq L_{Rfe} \\ \delta_1 & \text{for } \bar{L}_{Rfi}^{eq} > L_{Rfe} \end{cases} \quad (8.47)$$

$$\delta_{Li}(V_f^{tr}) = \delta_1 \cdot \left\{ 1 - \cos \left[ -\arcsin \frac{C_3}{\delta_1} \right] \right\} \quad (8.48)$$

$$V_{fi,eff}^{max} = V_{fi,eff}(\gamma_{max}) = \frac{\delta_1 \cdot A_2}{2 \cdot L_d \cdot A_3 \cdot \gamma_{max}} \cdot \left[ \frac{\pi}{2} - \arcsin \psi - \psi \cdot \sqrt{1 - \psi^2} \right] \quad (8.49)$$

$$A_2 = \frac{L_p \cdot \lambda}{J_1}; \quad A_3 = \frac{\sin(\theta + \beta)}{2 \cdot \delta_1}; \quad \gamma_{max} = \frac{2 \cdot \delta_{Lu}}{L_d \cdot \sin(\theta + \beta)}; \quad (8.50)$$

$$\psi = 1 - A_3 \cdot \gamma_{max} \cdot L_d$$

$$V_{fd} = \frac{1}{\gamma_{Rd}} \cdot V_f = \frac{1}{\gamma_{Rd}} \cdot \left( 2 \cdot N_{f,int}^l \cdot V_{fi,eff}^{max} \cdot \sin \beta \right) \quad (8.51)$$

The predictive performance of this model was assessed by Bianco et al. (2013) by using available experimental results. Assuming for the angle  $\alpha$  the value of  $28.5^\circ$  for all the experimental programs, considering for the  $f_{cm}$  the values determined from the formulae of the CEB-FIP Model Code 90 (1993), and adopting for the local bond stress-slip relationship the values  $\tau_0 = 20.1$  MPa and  $\delta_1 = 7.12$  mm, this formulation provided very satisfactory estimates of the experimental recordings, resulting the ratio of the prediction versus the experimental value characterized by a mean value and a standard deviation of 0.69 and 0.29, respectively.

**Acknowledgments** The first author would like to thank the support by FEDER funds through the Operational Program for Competitiveness Factors—COMPETE and National Funds through FCT—Portuguese Foundation for Science and Technology under the project CutInDur PTDC/ECM/112396/2009.

## References

- ACI (2008). Guide for the design and construction of externally bonded FRP systems for strengthening concrete structures. *Report by ACI Committee 440.2R-08*, American Concrete Institute, Farmington Hills, MI, USA, 76 pp.
- Alkhrdaji, T., Barker, M., Chen, G., Mu, H., Nanni, A., & Yang, X. (2001). Destructive and Non-Destructive Testing of Bridge J857, Phelps County, Missouri. Vol. III- Strengthening and Testing to Failure of Bridge Piers, Centre for Infrastructure Engineering Studies, University of Missouri at Rolla, Report No.RDT01-002C, 90 pp.
- Al-Mahmoud, F., Castel, A., François, R., & Tourneur, C. (2009). Strengthening of RC members with near-surface mounted CFRP rods. *Composite Structures*, 91(2), 138–147.
- Asplund, S. Q. (1949). Strengthening bridge slabs with grouted reinforcement. *ACI Journal*, 52(6), 397–406.
- Barros, J. A. O., & Dias, S. J. E. (2006). Near surface mounted CFRP laminates for shear strength-ening of concrete beams. *Journal Cement and Concrete Composites*, 28(3), 276–292.
- Barros, J. A. O., Dias, S. J. E., & Lima, J. L. T. (2007). Efficacy of CFRP-based techniques for the flexural and shear strengthening of concrete beams. *Cement & Concrete Composites*, 29(3), 203–217.
- Barros, J. A. O., & Fortes, A. S. (2005). Flexural strengthening of concrete beams with CFRP laminates bonded into slits. *Journal of Cement & Concrete Composites*, 27, 471–480.
- Barros, J. A. O., Varma, R. K., Sena-Cruz, J. M., & Azevedo, A. F. M. (2008). Near surface mounted CFRP strips for the flexural strengthening of RC columns: Experimental and numerical research. *Engineering Structures*, 30(12), 3412–3425.
- Bianco, V., Barros, J. A. O., & Monti, G. (2010). New approach for modeling the contribution of NSM FRP strips for shear strengthening of RC beams. *ASCE Composites for Construction Journal*, 14(1), 36–48.
- Bianco, V., Monti, G., & Barros, J.A.O. (2013). Design formula to evaluate the NSM FRP strips shear strength contribution to a RC beam. *Composites Part B: Engineering*.
- Bilotta, A., Ceroni, F., Di Ludovico, M., Nigro, E., Pecce, M., & Manfredi, G. (2011). Bond efficiency of EBR and NSM FRP systems for strengthening concrete members. *Journal of Composites for Construction*, 15(5), 757–772.
- Bilotta, A., Ceroni, F., Di Ludovico, M., Nigro, E., Pecce, M., & Manfredi, G. (2012). Experimental bond test on concrete members strengthened with NSM FRP systems: influence of groove dimensions and surface treatment. In *Proceedings of the CICE 2012, Rome, Italy* (p. 8).
- Blaschko, M. (2001). *Zum tragverhalten von betonbauteilen mit in schlitze eingeklebten CFK-lamellen. Bericht 8/2001 aus dem Konstruktiven Ingenieurbau (in German)*. Germany: TU München. 147 pp.
- Blaschko, M. (2003). Bond behaviour of CFRP strips glued into slits. In *Proceedings of the FRPRCS-6. Singapore: World Scientific* (pp. 205–214).
- Bonaldo, E. (2008). *Composite materials and discrete steel fibres for the strengthening of thin concrete structures*. Civil Engineering Department: University of Minho.
- Bonaldo, E., Barros, J.A.O., & Lourenço, P.B. (2008). Efficient Strengthening Technique to Increase the Flexural Resistance of Existing RC Slabs. *Journal of Composites for Construction*, 149–159.
- Bournas, D., Lontou, P., Papanicolaou, C. G., & Triantafillou, T. C. (2007). Textile-reinforced mortar (TRM) versus FRP confinement in reinforced concrete columns. *ACI Structural Journal*, 104(6), 740–748.
- Bournas, D. A., & Triantafillou, T. C. (2009). Flexural strengthening of RC columns with NSM FRP or stainless steel. *ACI Structural Journal*, 106(5), 495–505.
- Bournas, D. A., & Triantafillou, T. C. (2013). Biaxial bending of RC columns strength-ened with externally applied reinforcement combined with confinement. *ACI Structural Journal*, 110(2), 193–204.

- Burke, P.J. (2008). Low and high temperature performance of near surface mounted FRP strengthened concrete slabs. *MSc Thesis*, Department of Civil Engineering, Queen's University, 193 pp.
- Castro, E.K., Melo, G.S., & Nagato, Y. (2007). Flexural strengthening of RC "T" beams with near surface mounted (NSM) FRP reinforcements. In *Proceedings of the eight international conference on fibre-reinforced plastics for reinforced concrete structures (FRPRSCS-8)*, Patras, Greece.
- CEB-FIP Model Code 90 (1993). Bulletin d'Information N° 213/214. *Final version printed by Th. Telford*, London, 460 pp.
- Ceroni, F., Pecce, M., Bilotta, A., & Nigro, E. (2012). Bond behavior of FRP NSM systems in concrete elements. *Composites Part B Engineering*, 43(2), 99–109.
- Cholostiakow, S., Kotynia, R., & Przygocka, M. (2013). Flexural strengthening of reinforced concrete structures with near surface mounted FRP composites. In *Proceedings of the 9th Central European Congress on Concrete Engineering*, Wroclaw.
- Coelho, M., Sena-Cruz, J.M., & Neves, L.A.C. (2013). State of the art of bond tests with FRP NSM systems in concrete. Report no. 13-DEC/E-12, University of Minho, Guimarães, Portugal, 104 pp.
- Coelho, M., Sena-Cruz, J.M., & Neves, L.A.C. (2014). A review on the bond behavior of FRP NSM systems in concrete. *Submitted to Construction and Building Materials*.
- Costa, I. G., & Barros, J. A. O. (2010). Flexural and shear strengthening of RC beams with composite materials – The influence of cutting steel stirrups to install CFRP strips. *Cement & Concrete Composites*, 32, 544–553.
- Costa, I., & Barros, J. (2011). Assessment of the bond behaviour of NSM FRP materials by pullout tests. In *Proceedings of the First Middle East Conference on Smart Monitoring, Assessment and Rehabilitation of Civil Structures, Dubai, UAE* (p. 8).
- Dalfré, G. M. (2013). *Flexural and shear strengthening of RC elements*. Civil Engineering Department: University of Minho.
- Dalfré, G., & Barros, J. (2011). Assessing the effectiveness of a NSM-CFRP flexural strengthening technique for continuous RC slabs by experimental research. In *Proceedings of the First Middle East Conference on Smart Monitoring Assessment and Rehabilitation of Civil Structures (SMAR 2011)*, Dubai.
- De Lorenzis, L., Lundgren, K., & Rizzo, A. (2004). Anchorage length of near-surface mounted fiber-reinforced polymer bars for concrete strengthening — Experimental investigation and numerical modeling. *ACI Structural Journal*, 101(2), 269–278.
- De Lorenzis, L., & Nanni, A. (2002). Bond between near-surface mounted fiber-reinforced polymer rods and concrete in structural strengthening. *ACI Structural Journal*, 99(2), 123–132.
- De Lorenzis, L., Nanni, A., & La Tegola, A. (2000). Flexural and shear strengthening of reinforced concrete structures with near surface mounted FRP rods. In J. Humar & AG Razaqpur (Eds.), *Proceedings of the third international conference on advanced composite materials in bridges and structures, Ottawa, Canada* (pp. 521–528).
- De Lorenzis, L., Rizzo, A., & La Tegola, A. (2002). A modified pull-out test for bond of near-surface mounted FRP rods in concrete. *Composites Part B Engineering*, 33(8), 589–603.
- De Lorenzis, L., & Teng, J. G. (2007). Near-surface mounted FRP reinforcement: An emerging technique for strengthening structures. *Composites Part B Engineering*, 38(2), 119–143.
- Dias, S. J. E. (2008). *Experimental and analytical research on the shear strengthening of RC beams according to the NSM CFRP technique*. Ph.D. Departamento de Engenharia Civil: Universidade do Minho (in Portuguese). 391 pp.
- Dias, S. J. E., & Barros, J. A. O. (2012). NSM shear strengthening technique with CFRP laminates applied in high-strength concrete beams with or without pre-cracking. *Composites Part B: Engineering Journal*, 43(2), 290–301.
- Dias, S. J. E., & Barros, J. A. O. (2013). Shear strengthening of RC beams with NSM CFRP laminates: experimental research and analytical formulation. *Composite Structures Journal*, 99, 477–490.

- El-Hacha, R., & Rizkalla, S. (2004). Near-Surface-Mounted fiber-reinforced polymer reinforcements for flexural strengthening of concrete structures. *ACI Structural Journal*, 101(5), 717–726.
- El-Hacha, R., & Wagner, M. (2009). Shear strengthening of reinforced concrete beams using near-surface mounted CFRP strips. In *Proceedings of the 9th International Symposium on Fiber Reinforced Polymers Reinforcement for Concrete Structures (FRPRCS-9)*, Sydney, Australia (p. 10).
- En-Core and fib TG 9.3 (2010). Internal reports: Round robin testing exercise – universities of gent, minho and budapest. Retrieved from <http://cigroup.shef.ac.uk/encore/rtt/index.php>.
- fib (2001). Externally bonded FRP reinforcement for RC structures. In *Bulletin No. 14, International Federation for Structural Concrete, Lausanne, Switzerland* (138 pp).
- Galati, D., & De Lorenzis, L. (2009). Effect of construction details on the bond performance of NSM FRP bars in concrete. *Advances in Structural Engineering*, 12(5), 683–700.
- Hassan, T., & Rizkalla, S. (2003). Investigation of bond in concrete structures strengthened with near surface mounted carbon fiber reinforced polymer strips. *Journal of Composites for Construction*, 7(3), 248–257.
- Kalayci, A.S. (2008). *Development of surface flaw thresholds for pre-cured fiber reinforced polymer and groove size tolerance for near surface mounted fiber reinforced polymer retrofit systems*. Ph.D. Thesis, Department of Civil and Environmental Engineering, Florida International University, 160 pp.
- Kotynia, R. (2007a). Analysis of the flexural response of NSM FRP-strengthened concrete beams. In *Proceedings of the eight international conference on fibre-reinforced plastics for reinforced concrete structures (FRPRSCS-8)*. Patras, Greece.
- Kotynia, R. (2007b). Shear strengthening of RC beams with NSM CFRP laminates. In *Proceedings of the 8th International Symposium on Fiber Reinforced Polymer Reinforcement for Concrete Structures (FRPRCS-8)*. Patras, Greece.
- Liu, I. S. T., Oehlers, D. J., & Seracino, R. (2006). Tests on the ductility of reinforced concrete beams retrofitted with FRP and steel near-surface mounted plates. *Journal of Composites for Construction*, 10(2), 106–114.
- Maaddawy, T. E., & Dieb, S. E. (2011). Near-Surface-Mounted composite system for repair and strengthening of reinforced concrete columns subjected to axial load and biaxial bending. *ASCE Journal of Composites for Construction*, 15(4), 602–614.
- Novidis, D.G., & Pantazopoulou, S.J. (2007). Beam tests of NSM-FRP laminates in concrete. In *Proceedings of the eight international conference on fibre-reinforced plastics for reinforced concrete structures (FRPRSCS-8)*. Patras, Greece.
- Novidis, D. G., & Pantazopoulou, S. J. (2008). Bond tests of short NSM-FRP and steel bar anchorages. *Journal of Composites for Construction*, 12(3), 323–333.
- Palmieri, A., Matthys, S., Barros, J., Costa, I., Bilotta, A., Nigro, E., Ceroni, F., szabó, Z.K., & Balázs, G.L. (2012). Bond of NSM FRP strengthened concrete: round robin test initiative. In *Proceedings of the CICE 2012, Rome, Italy* (p. 8).
- Perrone, M., Barros, J. A. O., & Aprile, A. (2009). A CFRP-based strengthening technique to increase the flexural and energy dissipation capacities of RC column. *ASCE Journal of Composites for Construction*, 13(5), 372–383.
- Prota, A., Manfredi, G., Balsamo, A., Nanni, A., & Cosenza, E. (2005). Innovative technique for seismic upgrade of RC square columns. In *Proceedings of the FRPRCS-7 International Symposium, Kansas, USA* (pp. 1289–1304). ACI SP-230-73.
- Realfonzo, R., & Napoli, A. (2009). Cyclic behavior of RC columns strengthened by FRP and steel devices. *Journal of Structural Engineering*, 135(10), 1164–1176.
- Sena Cruz, J. M., & Barros, J. A. O. (2004). Bond between near-surface mounted carbon-fiber-reinforced polymer laminate strips and concrete. *Journal of Composites for Construction*, 8(6), 519–527.
- Sena Cruz, J., Barros, J., Gettu, R., & Azevedo, Á. (2006). Bond behavior of near-surface mounted CFRP laminate strips under monotonic and cyclic loading. *Journal of Composites for Construction*, 10(4), 295–303.

- Seracino, R., Jones, N. M., Ali, M. S. M., Page, M. W., & Oehlers, D. J. (2007). Bond strength of near-surface mounted FRP strip-to-concrete joints. *Journal of Composites for Construction*, 11(4), 401–409.
- Täljsten, B., Carolin, A., & Nordin, H. (2003). Concrete structures strengthened with near surface mounted reinforcement of CFRP. *AN International Journal*, 6(3), 201–213.
- Teng, J. G., De Lorenzis, L., Wang, B., Li, R., Wong, T. N., & Lam, L. (2006). Debonding failures of RC beams strengthened with near surface mounted CFRP strips. *Journal of Composites for Construction*, 10(2), 92–105.
- Triantafillou, T., & Antonopoulos, C. (2000). Design of concrete flexural members strengthened in shear with FRP. *Journal of Composites for Construction*, 4(4), 198–205.
- Vrettos, I., Kefala, E., & Triantafillou, T. C. (2013). Innovative flexural strengthening of RC columns using carbon spike anchors. *ACI Structural Journal*, 110(1), 63–70.
- Dias, S., Coelho, M., & Sena Cruz, J.M. (2011). Presentation on the 6th meeting of RILEM TC 234-DUC: NSM Systems.
- Yost, J. R., Gross, S. P., Dinehart, D. W., & Mildenberg, J. J. (2007). Flexural behavior of concrete beams strengthened with near-surface-mounted CFRP strips. *ACI Structural Journal*, 104(4), 430–437.